Pontifícia Universidade Católica
do Rio de Janeiro

Muhammad Saleh Hayat

Study of sulfates thermal decomposition under the presence of in-situ generated reducing agents

Dissertação de Mestrado

Dissertation presented to the Programa de Pós-Graduação em Engenharia Química, de Materiais e Processos Ambientais in partial fulfillment of the requirements for the degree of Mestre em Engenharia Química, de Materiais e Processos Ambientais

Advisor: Prof. Rogério Navarro Correia de Siqueira

Rio de Janeiro
April 2025

Pontifícia Universidade Católica
do Rio de Janeiro

Muhammad Saleh Hayat

Study of sulfates thermal decomposition under the presence of in-situ generated reducing agents

Dissertation presented to the Programa de Pós-graduação em Engenharia Química, de Materiais e de Processos Ambientais of PUC-Rio in partial fulfillment of the requirements for the degree of Mestre em Engenharia de Química, de Materiais e de Processos Ambientais. Approved by the undersigned Examination Committee.

Prof. Rogério Navarro Correia de Siqueira
Advisor
Departamento de Engenharia Química e de Materiais – PUC-Rio

Dr. Artur Serpa de Carvalho Rego
Co-Advisor
Departamento de Engenharia Química e de Materiais – PUC-Rio

Prof. Francisco José Moura
Departamento de Engenharia Química e de Materiais – PUC-Rio

Prof. Laurindo de Salles Leal Filho
Departamento de Engenharia de Minas de Petróleo – USP

Rio de Janeiro, April 14th, 2025

Muhammad Saleh Hayat

Graduated in Mining Engineering from the University of Engineering and technology, Lahore, Pakistan (Uet Lahore, Pakistan))

Bibliographic data

Hayat, Muhammad Saleh

Study of sulfates thermal decomposition under the presence of in-situ generated reducing agents / Muhammad Saleh Hayat ; advisor: Rogério Navarro Correia de Siqueira ; co-advisor: Artur Serpa de Carvalho Rego. – 2025.

82 f. ; 30 cm

Dissertação (mestrado)–Pontifícia Universidade Católica do Rio de Janeiro, Departamento de Engenharia Química e de Materiais, 2025.

Inclui bibliografia

1. Engenharia Química e de Materiais – Teses. 2. Sulfato de magnésio. 3. Sulfato de níquel. 4. Decomposição térmica. 5. Análise termogravimétrica. 6. Modelagem cinética. I. Siqueira, Rogério Navarro Correia de. II. Rego, Artur Serpa de Carvalho. III. Pontifícia Universidade Católica do Rio de Janeiro. Departamento de Engenharia Química e de Materiais. IV. Título.

CDD: 620.11

Acknowledgements

To my advisor, Professor Rogério Navarro Correia de Siqueira for the trust placed in me during this journey.

To my co-supervisor, Dr. Artur Serpa de Carvalho Rego, for his dedication and constant support and for the friendship developed during our time together.

To my parents, Muhammad Aslam and Zakia bibi, for all their dedication during my life and for showing me the importance of studies.

To my friends, for being present always and being a fundamental part of my day-to-day.

To the other professors of the Department of Chemical and Materials Engineering, for the knowledge transmitted to me during my journey in this institution.

To the employees of the Chemical and Materials Engineering Department, Carmem Façanha, Leonardo Rabello, Rosely Gonçalves and Matheus de Oliveira, for their attention.

To the technicians of the Chemical and Materials Engineering Department, Henrique Meira da Silva, and Vitor Hugo da Cunha, for the technical support provided to me and my project.

To the Pontifical Catholic University of Rio de Janeiro for the opportunity to study at an institution that values excellence in its teaching and research, while supporting students when necessary.

To Vale S.A., for the technical support, which made it possible to conceive and carry out this work

This study was financed in part by the Coordenação de Aperfeiçoamento de Pessoal de Nível Superior - Brasil (CAPES) - Finance Code 001.

Abstract

Muhammad Saleh Hayat; Rogério Navarro Correia de Siqueira (advisor), Artur Serpa de Carvalho Rego (Co-Advisor). **Study of sulfates thermal decomposition under the presence of in-situ generated reducing agents.** Rio de Janeiro, 2025. 82 p. Dissertação de mestrado - Department of Engineering Chemistry and Materials Pontifical Catholic University of Rio de Janeiro

This study investigates the thermal decomposition of magnesium sulfate heptahydrate ($MgSO_4 \cdot 7H_2O$) and nickel sulfate hexahydrate ($NiSO_4 \cdot 6H_2O$) using thermogravimetric analysis (TGA) and kinetic modeling. The experiments were performed on 10 mg samples with different stoichiometric ratio of sulfate to in-situ generated reducing agent, employing graphite and sugarcane bagasse as reductants. TGA results for pure $MgSO_4 \cdot 7H_2O$ revealed three dehydration stages, leading to an anhydrous state at 300°C, stability until 950°C, and decomposition into MgO at 1050°C. Graphite reduced the decomposition onset temperature to 900°C, while sugarcane bagasse had minimal influence. For $NiSO_4 \cdot 6H_2O$, dehydration occurred up to ~300°C, with complete decomposition into NiO at 820°C. Graphite lowered the decomposition onset by 120–200°C, while sugarcane bagasse induced a minor shift to 300°C due to volatile release. Kinetic analysis showed that the activation energy (Ea) for pure $MgSO_4 \cdot 7H_2O$ was 321.93 $kJ \cdot mol^{-1}$, decreasing significantly to 82.62 $kJ \cdot mol^{-1}$ with 10% graphite. With increasing graphite content, Ea values were 100.23 $kJ \cdot mol^{-1}$ (80%-20%) and 101.82 $kJ \cdot mol^{-1}$ (70%-30%), indicating a saturation effect. The reaction order was 1.36, suggesting a chemically controlled process. For $NiSO_4 \cdot 6H_2O$, Ea dropped from 130.045 $kJ \cdot mol^{-1}$ (pure) to 82.62 $kJ \cdot mol^{-1}$ with a 70%-30% graphite mixture, whereas sugarcane bagasse resulted in a modest reduction to 123.74 $kJ \cdot mol^{-1}$.These findings underscore the significant role of carbon-based reducing agents in modifying sulfate decomposition behavior. Graphite demonstrated a strong catalytic effect, reducing decomposition temperatures and activation energy, thereby enhancing energy efficiency in sulfate processing.

Keywords: Sugarcane bagasse; Metal sulfate; Termogravimetry; Kinetic modelling.

Resumo

Muhammad Saleh Haya-Rogério Navarro Correia de Siqueira (orientador), Artur Serpa de Carvalho Rego (Coorientador). **Estudo da decomposição térmica de sulfatos na presença de agentes redutores gerados in-situ**. Rio de Janeiro, 2025. 82 p. Dissertação de mestrado - Departamento de Engenharia Química e de Materiais, Pontifícia Universidade Católica do Rio de Janeiro

Este estudo investiga a decomposição térmica do $MgSO_4 \cdot 7H_2O$ e do $NiSO_4 \cdot 6H_2O$ por análise termogravimétrica (TGA) e modelagem cinética, utilizando grafite e bagaço de cana como agentes redutores. Para o $MgSO_4 \cdot 7H_2O$, foram observados três estágios de desidratação até o estado anidro em ~300°C, estabilidade até 950°C e decomposição em MgO a 1050°C; o grafite reduziu a temperatura inicial para ~900°C, enquanto o bagaço teve efeito mínimo. O $NiSO_4 \cdot 6H_2O$ desidratou até ~300°C e se decompôs em NiO a ~820°C; o grafite antecipou a decomposição entre 120–200°C, e o bagaço deslocou levemente para ~300°C devido a voláteis. A energia de ativação (Ea) para o $MgSO_4 \cdot 7H_2O$ caiu de 321,93 $kJ \cdot mol^{-1}$ (puro) para 82,62 $kJ \cdot mol^{-1}$ com 10% de grafite, estabilizando em ~100 $kJ \cdot mol^{-1}$ em proporções maiores; a ordem de reação (~1,36) indicou controle químico. Para o $NiSO_4 \cdot 6H_2O$, a Ea diminuiu de 130,05 $kJ \cdot mol^{-1}$ (puro) para 82,62 $kJ \cdot mol^{-1}$ (70%-30% grafite), enquanto o bagaço reduziu modestamente para 123,74 $kJ \cdot mol^{-1}$. Os resultados evidenciam o papel catalítico do grafite, reduzindo temperaturas e Ea, e destacam a relevância de redutores à base de carbono para maior eficiência energética no processamento de sulfatos.

Palavras-chave:

Bagaço de cana de açúcar; Sulfatos metálicos; Termogravimetria; Modelagem Cinética.

Table of Contents

List of Figures

List of Tables

1. Introduction

1.1. Context

Magnesium, an essential element in various industrial and biological processes, occurs abundantly in seawater, minerals, and brines. It ranks as the eighth most plentiful element in the Earth's crust and the third most abundant dissolved element in seawater. This abundance underscores its significance in natural and industrial systems. Magnesium is a grayish metal known for its strong reactivity and distinct properties. When burned, it emits an intense bright white glow, a feature utilized in applications such as fireworks, flares, and photography lighting. Magnesium belongs to the alkaline earth metal group, sharing characteristics such as high reactivity and the ability to form stable compounds with oxygen and water.(1,2,3) The historical development of magnesium production highlights its industrial importance. In 1808, Sir Humphry Davy first isolated magnesium by electrolyzing magnesium chloride. This method marked the advent of magnesium extraction using electrolysis, a process that remains foundational to its production. Industrial-scale manufacturing began in 1886, leveraging advancements in electrolysis techniques to produce metallic magnesium.(3)

The main source of magnesium in Brazil is magnesite; another mineral widely used in the world as a source of magnesium is dolomite (4,5). Magnesite ($MgCO_3$) has approximately 29% (w/w) of the mass related to magnesium, while dolomite [$CaMg(CO_3)_2$] has 13% magnesium in its structure. According to the Web mineral database, there are more than 230 minerals cataloged containing at least 10% by mass composed of magnesium in their structures, several of which contain other metals and serve as a source for processing these metals.

Hydrated magnesium sulfate can either be dried first (in the case of heptahydrate) or decomposed directly into magnesium oxide and sulfur dioxide, which can be used as a neutralizing agent in the leaching process and for the production of sulfuric acid, respectively. The advantage is that the waste products of the hydrometallurgical process are recycled internally instead of being disposed of, which also lowers the need for feed materials such as neutralizing agents and acid into the

process. Not only is this beneficial from an economic point of view, it also reduces the environmental footprint of the plant.(6) A general flowsheet to illustrate this process is shown in Figure 1. It is advantageous to use magnesium sulfate with low crystal water content as the feed material, as the energy requirement for dehydration will be lower and the sulfur dioxide content in the off gas will be less diluted.

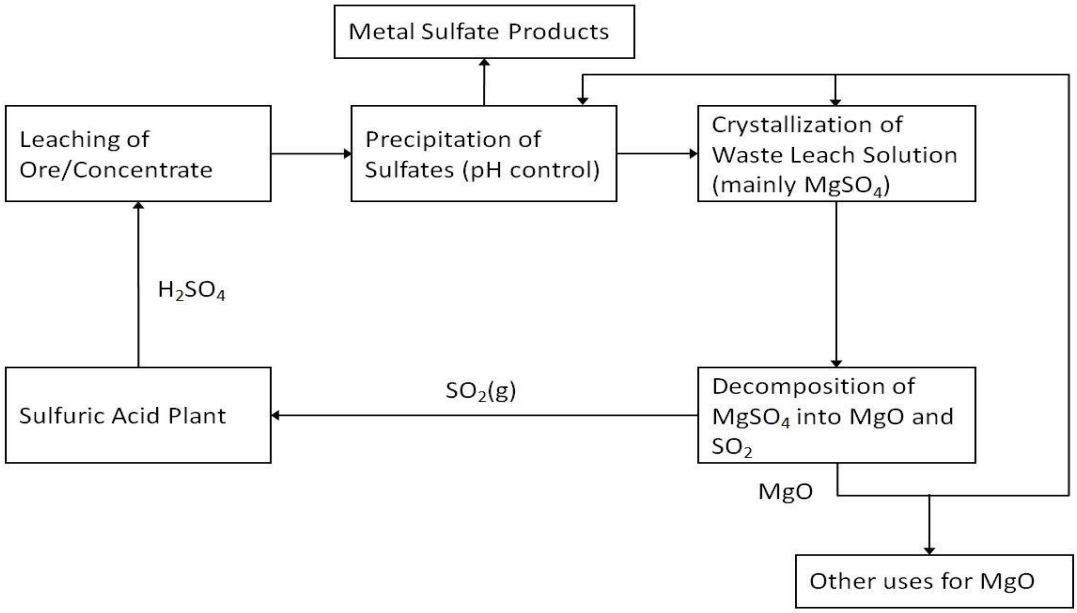

Figure 1. General flowsheet for a hydrometallurgical treatment process and the recycling of magnesium oxide and sulfur to the process.

When heated, magnesium sulfate hydrates release their crystalline water, transitioning to anhydrous magnesium sulfate. This process is represented by Eq. (1). However, the reported temperature for complete dehydration varies in the literature, with some studies indicating temperatures exceeding 300°C (7), while others suggest 320°C (8), 330–380°C(9), or even as high as 400–500°C (10). The dehydration process, particularly for higher hydrates like epsomite ($MgSO_4.7H_2O$), often occurs in distinct stages, producing intermediate hydrates with varying water content, such as $MgSO_4.6H_2O$, $MgSO_4.4H_2O$, $MgSO_4.3H_2O$, $MgSO_4.2H_2O$, $MgSO_4.1.25H_2O$, and $MgSO_4.H_2O$.(10) These transformations are influenced by external factors, such as temperature and atmosphere conditions, which can lead to the formation of metastable hydrates, making dehydration more difficult. Emons et al. (9) reported that the stepwise dehydration of epsomite yields stable intermediate hydrates, including $MgSO_4.3H_2O$ at

105°C, $MgSO_4.2H_2O$ at 140°C, and $MgSO_4.H_2O$ at 190°C. Unlike natural kieserite, which dehydrates in a single step, synthetic kieserite ($MgSO_4.1.25H_2O$) gradually loses its crystalline water. These variations in dehydration behavior underline the complexity of magnesium sulfate hydrates and highlight the influence of both natural and synthetic conditions on their thermal stability and structural transformations.

$$MgSO_4.xH_2O \leftrightarrow MgSO_4 + xH_2O \quad (1)$$

Nickel sulfate can crystallize as hydrated salts with different hydration levels, ranging from monohydrate to heptahydrate, depending on the reaction temperature. Under neutral conditions, crystallization between 5°C and 100°C primarily leads to the formation of hexahydrate ($NiSO_4·6H_2O$) and heptahydrate ($NiSO_4·7H_2O$), making them the most commonly studied phases.(11) The hexahydrate form exists in two polymorphs: α-$NiSO_4·6H_2O$ (retgersite) and β-$NiSO_4·6H_2O$, which differ in their structural stability and formation conditions.(12) During roasting, nickel sulfate can decompose into nickel oxide depending on the experimental conditions. A protective layer of $NiSO_4$ often forms on the oxide surface, inhibiting further sulfation. However, this passivating layer can be effectively removed through temperature cycling, allowing the reaction to proceed. In air, roasting nickel sulfide can yield either nickel sulfate or nickel oxide, depending on parameters such as temperature and gas composition. Due to the varying thermal stabilities of metal sulfates and oxides, selective sulfation and oxidation roasting offer potential for separating individual components from complex mineral mixtures.(13)

An example of potential biomass is sugarcane bagasse, which is composed of the fibrous residue of sugarcane after it has gone through the grinding process for extracting juice for fermentation and production of ethanol. The ethanol plant typically uses part of this waste to generate heat and power for itself (14,15), but such use is still lower than the generation of bagasse, and a significant portion of the bagasse is stored. The latter has low economic value and constitutes an environmental problem for production units.

1.2 Justification and Relevance

The decomposition reaction of $MgSO_4$ into MgO can be conducted under different operating conditions, making it essential to establish a comprehensive literature base. Numerous studies have focused on the thermodynamic aspects of $MgSO_4$ thermal decomposition, providing valuable insights into reaction feasibility and stability under various conditions.(16,6,17,18)However, when it comes to the reducing thermal decomposition of $MgSO_4$, especially the ones conducted under oxidizing conditions have explored this process in depth. Despite this, the available research provides a solid theoretical foundation for further investigation.

The thermal decomposition of $NiSO_4$ into NiO can occur under a variety of operating conditions, highlighting the need for a well-established literature base. Numerous studies have addressed the thermodynamic behavior of $NiSO_4$, offering valuable insights into its phase stability and decomposition pathways under different temperature and atmospheric conditions. While most research has focused on its decomposition in oxidizing environments such as air, limited work has been done under reducing or inert atmospheres.(13,19,20) Nevertheless, the available literature provides a strong theoretical foundation for further exploration. Understanding the decomposition behavior of $NiSO_4$ is particularly important for its practical applications, including nickel extraction, selective sulfation roasting, catalyst preparation, and the recovery of valuable components from nickel-bearing materials.

While thermodynamic studies on $MgSO_4$ and $NiSO_4$ decomposition are well-documented, the kinetic analysis of this reaction has received significantly less attention in the literature. The limited available studies on the kinetics of $MgSO_4$ and $NiSO_4$ decomposition often focus on only one or two specific reaction systems without broader comparative analysis. (21,22,23,16) Given this gap in research, there is a strong need for a more comprehensive kinetic evaluation under different reaction conditions, particularly in the presence of reducing agents such as graphite and sugarcane bagasse.

Therefore, this study aims to contribute to the theoretical foundation of $MgSO_4$ and $NiSO_4$ decomposition by conducting a detailed kinetic and

thermodynamic analysis under diluted air atmosphere (Air + N_2), and 10,20,30 wt.% Graphite and Sugarcane bagasse mixture with 90,80,70 wt.% magnesium sulfate heptahydrate ($MgSO_4.7H_2O$) and Nickel sulfate hexahydrate ($NiSO_4.6H_2O$). By evaluating different variables and comparing multiple reaction systems, this work seeks to provide a deeper understanding of the role of reducing agents in the thermal decomposition process, ultimately expanding the current scientific knowledge on this topic. This work seeks to understand the effect of these additives on the thermal behavior and decomposition kinetics of magnesium sulfate.

1.3. Objective

1.3.1. General

This study aimed to investigate the kinetic and thermodynamic factors influencing the thermal decomposition of magnesium and nickel sulfate. The analysis focused on the effects of reducing agents, mixture proportions, and the degree of hydration. A systematic experimental approach was adopted to evaluate these factors progressively.

This study was proposed to evaluate the reaction system gradually, and therefore the experiments were carried out to describe an evaluative line.

1.3.2. Specifics

- Graphite and sugarcane are the carbon sources. The sugarcane, sourced from street vendors, was washed, dried, and shredded to enhance its reactivity, while graphite was finely ground to maximize its surface area.
- Carry out thermogravimetric tests, within a temperature range 25 to 1300 °C and with a single heating rate °C.min^{-1}, to evaluate the influence of two different carbon sources such as graphite and sugarcane bagasse on the thermal decomposition behavior of magnesium sulfate heptahydrate and nickel sulfate hexahydrate under diluted air atmosphere (Air + N_2).
- Apply the data obtained in thermogravimetric tests to a mathematical empirical model to obtain kinetic parameters and thereby contribute to the discussions proposed in this work.

1.4 Thesis Outlines

This thesis explores the thermal decomposition of magnesium sulfate through five chapters, covering the introduction, literature review, methodology, results, and conclusions.

2. Literature Review

2.1. Carbon and Carbon Sources

Research in the field of thermal decomposition has increasingly focused on strategies to lower the decomposition temperature and regulate the size of oxide particles. One approach involves optimizing the leaching process under diverse conditions, such as varying the composition in inert atmosphere and incorporating reducing agents.(17,24) These strategies aim to improve the efficiency of material processing while maintaining control over the properties of the resulting products(21,25)

In the minerals and metals processing sector, biomass has emerged as a promising alternative to traditional reductants like coal. the main advantage of using biomass is that the reducing agent can be produced in situ and has a sustainable nature, as its primary source is of biological origin. At elevated temperatures, biomass undergoes thermal decomposition to produce a range of byproducts, including char, hydrogen, methane, carbon monoxide, carbon dioxide, and other light hydrocarbons under inert atmosphere.(26) These byproducts can act as reducing agents, contributing to the reduction of metal oxides and other compounds in high-temperature processes. The use of biomass not only aligns with global sustainability goals but also offers the advantage of generating multifunctional reducing agents in situ, which can simplify processing pathways.

Carbon, on the other hand, remains a versatile and widely utilized reducing agent due to the extensive range of carbon-based compounds available. This diversity enables its application across various types of reduction processes, whether in solid-solid, solid-gas, or gas-gas systems. In solid-solid systems, carbon is typically employed in forms such as charcoal, graphite, and coke, which are readily available and provide consistent performance in metallurgical processes. These solid forms of carbon are particularly effective in high-temperature reduction reactions.(26,27)

For processes involving solid-gas or gas-gas systems, carbon compounds such as carbon monoxide (CO), and methane (CH_4) are frequently utilized as reducing agents. These gaseous forms of carbon are advantageous due to their ability to penetrate

reaction zones more effectively than solid reductants, ensuring uniform reduction across the material being processed. Carbon monoxide is a highly efficient reductant due to its strong affinity for oxygen, which allows it to effectively reduce metal oxides to their elemental or lower oxidation states. Methane, a hydrocarbon, also plays a dual role as both a reductant and a potential source of energy, further enhancing its appeal in industrial applications.(28,29) The combination of these reducing agents—biomass-derived products and various carbon forms—offers a comprehensive toolkit for optimizing reduction processes. The choice of reductant and its specific application depends on several factors, including the type of material being processed, the desired properties of the final product, and the economic and environmental considerations of the process. Biomass, for example, not only serves as a renewable reductant but also contributes to the circular economy by utilizing agricultural or forestry residues that would otherwise go to waste. (29)Similarly, the versatility of carbon compounds enables their integration into both traditional and innovative processing technologies, supporting advancements in materials science and engineering.

2.2 Sugarcane Bagasse Thermal behavior

Kumar et al.(30) conducted studies on thermogravimetric analysis (TGA) to compare the weight loss of different types of bagasse. They reported the highest TGA weight loss for nickel-impregnated bagasse (86 wt.%), while raw bagasse exhibited the lowest weight loss at 76.36 wt.%. Other impregnated variants, such as ruthenium and iron-impregnated bagasse, showed intermediate values of 83 wt.% and 79 wt.% losses, respectively, at a heating rate of 10 °C.min^{-1}. This work highlights the potential of impregnated biomass in improving the efficiency of thermal decomposition processes.

The thermal degradation of untreated, alkali-treated, and sulfuric acid-treated sugarcane bagasse was evaluated using non-isothermal thermogravimetric analysis under a nitrogen atmosphere. Both alkali and sulfuric acid treatments altered the initial chemical composition and structure of untreated SB. The alkali-treated sample exhibited higher thermal stability, whereas the acid-treated sample showed a change in degradation behavior around 40% mass loss.(31)

The thermo kinetics of the co-pyrolysis of two different types of coal biomass blends have been investigated via non-isothermal thermogravimetric analysis. The individual devolatilization behavior of each of the fuels used – coal, sugarcane bagasse and corn residue –was compared with the behavior of coal–biomass blends in order to identify synergistic behavior that points to the existence of chemical interactions between the coal and biomass fraction of the blends. The devolatilization of the biomass materials occurred in a narrow temperature interval (200–400 °C) and with higher decomposition rates than coal, of which the decomposition occurred between 380 and 900 °C.(32)

2.3. Thermal Decomposition of Sulfate

Hoteit et al.(33) reported that a low-oxygen atmosphere significantly reduces reaction temperatures, making it advantageous for various thermal processes. This effect can be explained by considering the role of oxygen in combustion and thermal decomposition reactions. In an oxygen-rich environment, exothermic oxidation reactions occur more readily, leading to higher reaction temperatures. However, when oxygen availability is limited, the extent of oxidation decreases, resulting in lower energy release and subsequently lower reaction temperatures.

Mostashari et al(34) focuses on the thermogravimetric analysis of cellulose cotton fabric treated with nickel sulfate hexahydrate ($NiSO_4 \cdot 6H_2O$) in a temperature range 25°C to 600°C under inert atmosphere. The untreated cotton displayed rapid decomposition at 330 °C, losing 98% of its mass by 500 °C. The treated cotton, however, showed significant mass loss starting at 250 °C, with the major mass loss occurring at 340 °C, where about 70% of the untreated cotton's mass was lost. The hydrated salt lost its water before the cellulose degradation zone, while the treated cotton lost most of its mass, including hydration water, within the cellulose degradation range. This indicates that the flame-retardant action of $NiSO_4 \cdot 6H_2O$ occurs by releasing hydration water during cellulose degradation.

The thermogravimetric analysis (TGA) and differential thermal analysis (DTA) of $NiSO_4 \cdot 6H_2O$ were conducted under air and helium atmospheres at a heating rate of 10 K/min. The DTA curve revealed four distinct endothermic effects,

corresponding to different thermal events occurring during heating. To investigate these effects, the samples were heated for 4 hours at specific temperatures of 383 K, 423 K, 473 K, 533 K, 773 K, and 1173 K. These temperatures were selected based on the DTA results, which indicated significant thermal transitions at these points. The TGA curve likely shows a stepwise mass loss due to the dehydration of $NiSO_4 \cdot 6H_2O$, with water molecules being released below 533 K, followed by the decomposition of anhydrous $NiSO_4$ at higher temperatures. Around 773 K, the compound may start decomposing further, leading to the evolution of SO_3 gas and the formation of NiO. At 1173 K, the material is expected to reach thermal stability, primarily consisting of NiO as the final solid residue.(19)

Ding et al. (35) analyzed the decomposition of $MgSO_4$ in the presence of natural gas, aiming to form H_2S, CO_2, and MgO. They found that H_2O can initiate the thermodynamic reduction of sulfate by promoting redox reactions. Water vapor may dissociate at high temperatures, generating hydrogen radicals or reacting with carbon-based species to form H_2 and CO, which enhance sulfate reduction. Additionally, H_2O alters gas-phase equilibria, lowering the decomposition temperature and influencing reaction kinetics, ultimately facilitating a more efficient reduction of $MgSO_4$.

Brownell et al (36) evaluated the reaction of anhydrous magnesium sulfate with silica, likely aiming to investigate the feasibility of MgSO4 reacting with silica under high-temperature conditions. However, they found that significant sulfate decomposition occurred from 1173 K onwards, preventing the intended reaction. Ostroff and Sanderson (1959) obtained a decomposition temperature for anhydrous $MgSO_4$ of 1168 K.

Straszko et al(20) studied the thermal decomposition of $NiSO_4 \cdot 6H_2O$ in air using TGA, revealing a stepwise mass loss pattern. The process began at 362 K with the loss of two water molecules (13.4% mass loss), followed by three more at 420 K (19.9%) and the final one at 613 K (6.6%), forming anhydrous $NiSO_4$. Decomposition of $NiSO_4$ started above 570 K, leading to NiO formation at 1083 K (total mass loss 29.7%). The DTA curve showed endothermic peaks at 391 K, 420 K, 613 K, and 1060 K, corresponding to dehydration and decomposition stages.

Souza et al. (25)studied the thermal decomposition of $MgSO_4$ with charcoal as a reducing agent to produce MgO within the temperature range of 600–900 °C under the inert temperature. Their work demonstrated that the use of charcoal significantly influences the decomposition process, offering a practical method to lower the temperature 777°C required for the formation of MgO.

Scheidema and Taskinen et al (17) investigated the stability of magnesium sulfate under different atmospheric conditions. Their thermodynamic analysis revealed that the presence of reducing gases—H_2, S_2, and CO—significantly lowered the initial decomposition temperature from 1085°C to 592°C, 623°C, and 606°C, respectively. These findings highlight the critical role of atmospheric composition in thermal decomposition. The initial gaseous phase likely consisted of $MgSO_4$ vapor along with the reducing gases in controlled ratios.

Tomaszewich E, et al(19) presented the DTA/TG curves recorded while heating the samples of $NiSO_4 \cdot 6H_2O$ in the atmosphere of air and of helium, at a heating rate of 10 K min^{-1}. The result found that temperature Ranges for decomposition typically occurred over a wide range, with specific stages for hydration loss and thermal breakdown. Dehydration began around 110°C, followed by further decomposition stages at 200-260°C. The final decomposition step occurred at temperatures as high as 810 °C.

King M, et al(37) investigated thermal decomposition of $NiSO_4 \cdot 6H_2O$, $NiC_{l2} \cdot 6H_2O$, and Ni $(SO_3NH_2)_2 \cdot xH_2O$ in 50–1200 °C range by simultaneous thermogravimetry (TG) and differential scanning calorimetry (DSC) in flowing air. The nickel salt hydrates first dehydrate in 100–350 °C, followed by decomposition into nickel oxide and gaseous species. The decomposition temperatures of the anhydrous $NiSO_4$, $NiCl_2$, and Ni $(SO_3NH_2)_2$ are, respectively, 810 °C, 740 °C, 375–797 °C.

Vekes B, et al(38) investigate the performance of Nickel-Cerium/HZSM-5 catalyst on pyrolysis of sugarcane bagasse and kinetic analysis via thermogravimetric analyzer. The sample is pyrolyzed from 30 to 700 °Cat multiple heating rates (5, 10, 20, and 30 °C/min) in a nitrogen environment. The HZSM-5 was used as a support,

while nickel and cerium were impregnated as promoters via incipient wetness impregnation method.

2.4 Kinetics of Thermal decomposition process

Kinetic data plays a fundamental role in understanding the mechanisms of chemical processes and optimizing reaction conditions. Numerous researchers have conducted experimental studies to explore the thermal decomposition kinetics of metal sulfates, which provide valuable insights into the behavior of these compounds under various conditions. These studies have focused on determining activation energy (Ea.) and reaction models, which are crucial for understanding the decomposition mechanisms and their dependence on temperature, atmosphere, and reducing agents.(39,40,41)

For thermogravimetric curves, kinetic modeling can obtain kinetic parameters for both isothermal and dynamic methods. Monteiro et al(42) that for the modeling of isothermal methods, several thermogravimetric graphs are needed, while for dynamic methods a single curve is capable of providing the data necessary for modeling.

Vachuška and Vobořil at al(43) in 1971 developed an algorithm designed for analyzing data from non-isothermal thermogravimetric curves, accounting for the thermal effects of reactions that cause deviations from the programmed heating profile of the samples. This algorithm was utilized to calculate the activation energy (Ea) and reaction order. The method was validated using data from the literature on the dehydration of gypsum and calcium oxalate monohydrate. The results showed excellent agreement with previously reported values in the literature.

2.4.1 Sulfate Decomposition Kinetic modelling

Straszko et al(20) used the Coats–Redfern method to analyze $NiSO_4 \cdot 6H_2O$ decomposition kinetics. The dehydration followed the random nucleation model (F1), while anhydrous $NiSO_4$ decomposition was best described by the three-dimensional diffusion (D^3) or contracting volume (R^3) models. The activation energy (Ea) for $NiSO_4$ decomposition was 269 kJ/mol, differing from the previously reported 236 kJ/mol.

Thermodynamic parameters were also evaluated, confirming that anhydrous $NiSO_4$ decomposed at the slowest rate.

Hulbert et al. (21) investigated the breakdown kinetics of anhydrous magnesium sulfate ($MgSO_4$) within the temperature range of 920 °C to 1080 °C under inert atmosphere. Using the contracting sphere model, they determined an activation energy of 311.7 $kJ \cdot mol^{-1}$ at 1020 °C. This study provided a detailed analysis of the decomposition mechanism, highlighting the influence of temperature on the reaction kinetics.

Vekes B, et al(38) investigate the performance of Nickel-Cerium/HZSM-5 catalyst on pyrolysis of sugarcane bagasse and kinetic analysis via thermogravimetric analyzer. The kinetic analysis of non-catalytic and catalytic pyrolysis was performed using the Flynn-Wall-Ozawa and Coats-Redfern methods. The catalytic pyrolysis has achieved higher activation energy (2.87 – 68.92 kJ/mol) over conversion than the non-catalytic pyrolysis (24.20 – 122.33 kJ/mol) using the Flynn-Wall-Ozawa method. The reaction mechanism of non-catalytic and catalytic pyrolysis follows power law (n=1) and chemical reaction (n=2) respectively via the Coats-Redfern method.

Plewa and Steindor (16) extended this investigation by conducting isothermal experiments on the decomposition of $MgSO_4$ in the presence of carbon monoxide (CO) within a narrower temperature range of 640 °C to 665 °C under oxidizing atmosphere. Employing the shrinking-core model, they determined an activation energy of 209.7 $kJ \cdot mol^{-1}$. The shrinking-core model assumes that the reaction occurs at the interface between the unreacted core and the reacted outer shell, making it particularly useful for reactions involving solid reactants and gaseous products. Their findings emphasized the significant role of CO as a reducing agent in lowering the energy barrier for the decomposition reaction, thereby improving process efficiency.

Mello et al. (44) investigated the catalytic effect of Pd/Al_2O_3 on the decomposition of magnesium sulfate under inert atmosphere. Their work demonstrated a substantial reduction in activation energy from 368.2 $kJ \cdot mol^{-1}$ to 258.8 $kJ \cdot mol^{-1}$ when

the catalyst was employed. This reduction highlights the potential of catalysts in facilitating thermal decomposition processes by lowering the energy requirements and enhancing reaction rates. The use of Pd/Al_2O_3 as a catalyst not only improved the decomposition kinetics but also provided a practical approach to optimize industrial processes involving magnesium sulfate.

Souza et al. (45) explored the thermal decomposition kinetics of hydrated magnesium sulfate ($MgSO_4.H_2O$) and demonstrated that the choice of reducing agent significantly influenced the activation energy under the inert atmosphere. Their study revealed that the activation energy decreased from 422.7 $kJ \cdot mol^{-1}$ for pure sulfate to 340.3 $kJ \cdot mol^{-1}$ with green coke, 196.1 $kJ \cdot mol^{-1}$ with graphite, 191.1 $kJ \cdot mol^{-1}$ with coke breeze, and 162.3 $kJ \cdot mol^{-1}$ with charcoal. The researchers utilized the Vachuska-Voboril (43)and Speyer model(46) to analyze their data, which provided a comprehensive framework for understanding the effect of reducing agents on the decomposition process. The findings underscore the importance of selecting appropriate reducing agents to enhance decomposition efficiency and reduce energy consumption in industrial applications.

Rueda et al (47)investigated the kinetics of the thermal decomposition reaction of sugarcane bagasse. Thermal decomposition experiments were conducted at four heating rates (1.25, 2.5, 5, and 10 °C/min) in a thermogravimetric analyzer under a nitrogen atmosphere. The kinetic analysis was performed using the isoconversional Friedman method, yielding activation energy values ranging from 154.1 kJ/mol to 177.8 kJ/mol. The reaction model was determined through master plots, corresponding to a two-dimensional diffusion mechanism. The pre-exponential factor was calculated as 1.82×10^9 s^{-1} by linearizing the conversion rate equation as a function of the inverse absolute temperature, with an activation energy of 149.7 kJ/mol, which is consistent with reported biomass thermal decomposition values.

Kumar el al(30) pyrolytic behavior, kinetics, and thermodynamics of raw and metal (Ni, Ru, Fe) impregnated sugarcane bagasse were analyzed using isoconversional models (FWO, KAS, Kissinger's) at heating rates of 5–20 °C/min.

Nano-metals (10–20 nm) formed oxides/hydroxides within the lignocellulosic matrix, reducing activation energy (SB-Ni: 62.50 kJ·mol^{-1}, SB-Ru: 78.46 kJ·mol^{-1}, SB-Fe: 83.09 kJ·mol^{-1}).

Huang et al(48) studied the effect of biomass on pyrolysis degradation of plastic wastes, poly (lactic acid) (PLA) has thus been attempted in present work to study the influence of sugar cane bagasse (SCB) on its pyrolysis behaviors and kinetic paramerizations. Using pyrolysis results, activation energies of Ea are isoconversionally calculated by applying differential Friedman, integral Kissinger-Akahira-Sunose, Flynn-Wall-Ozawa, Starink and Vyazovkin-Dollimore methods, resulting in 113.7 ~ 141.7, 101.3 ~ 140.4 and 79.8 ~ 210.1 kJ·mol^{-1} for the PLA blends with 10, 20 and 30 mass% of SCB

Collectively, these studies highlight the diverse approaches and methodologies used to investigate the thermal decomposition and reduction kinetics of metal sulfates and related compounds. The contracting sphere and shrinking-core models provide valuable tools for analyzing solid-state reactions, while the use of catalysts and reducing agents offers practical strategies to lower activation energies and improve reaction rates. The integration of biomass as a sustainable reducing agent further emphasizes the potential for environmentally friendly solutions in metallurgical and chemical processing.

3. Materials and Methods

3.1. Chemicals

In this study, Magnesium Sulfate Heptahydrate ($MgSO_4.7H_2O$), Nickel sulfate hexahydrate ($NiSO_4.6H_2O$) a crystalline compound widely used in chemical and industrial processes, was procured from Merck, a reputable supplier of high-purity analytical-grade chemicals. Graphite was purchased by Merck and it was synthetic carbon material while sugarcane bagasse was obtained from street vendors, was washed, dried, and shredded to improve its reactivity, while graphite was ground into a fine powder to increase its surface area. Both materials, were used as carbon sources during the sulfate decomposition process, enabling the in-situ generation of reducing agent, for example, carbon monoxide (CO) in the case of graphite.

3.2. Characterization

The characterization of both graphite and sugarcane bagasse was conducted through a single analysis: proximate composition analysis. This analysis followed the standard methods, including moisture content determination (ASTM E871–82), volatile matter content (ASTM E872–82), and fix carbon content (ASTM E1755–01).

3.3. Thermodynamics Assessment

Thermodynamic simulations were carried out to gain a deeper understanding of the reaction pathways and the formation of intermediate phases during the thermal treatment of $MgSO_4.7H_2O$, and $NiSO_4.6H_2O$. Simulations were performed using HSC Chemistry 10[56], considering 1.0 kmol of each hydrated sulfate and under varying amounts of carbon under oxidative atmosphere, as displayed in table 1. The temperature range for the analysis spanned from 25°C to 1300°C, covering typical conditions for thermal decomposition.

Table 1. Initial conditions for simulations with HSC under oxidative atmosphere.

Solid phase/species	**Pure Sulfate (Kmol)**	**90%Sulfate/10%Graphite mixture (Kmol)**
Solid phase		
$MgSO_4.7H_2O$	1.00	1.00
$NiSO_4.6H_2O$	1.00	1.00
Carbon (graphite) with $MgSO_4.7H_2O$		2.28
Carbon (Graphite) With $NiSO_4.6H_2O$		2.78
Gas Phase		
O_2 with $MgSO_4.7H_2O$	1	1
O_2 with $NiSO_4.7H_2O$	1	1
N_2	1.7	1.7

3.4. Thermogravimetric analysis

The operating conditions of the thermogravimetric analysis were by a temperature range of 25-1300 °C, a heating rate of 10 °C.min^{-1}, and sample mass of 10 mg. Samples consisted of pure sulfates or mixtures with the sulfate and the carbon bearing phase (graphite or sugarcane bagasse), under different proportions (Table 2).

All thermogravimetric tests were performed on the Netzsch STA 449 F3 Jupiter® under diluted air atmosphere, available in the Department of Chemical and Materials Engineering of the Pontifical Catholic University of Rio de Janeiro (DEQM/PUC-Rio).

Table 2. Composition of the samples used in the present study

Experiment	Sulfate sample	Reducing agent
1	$MgSO_4.7H_2O$	-
2	$MgSO_4.7H_2O$ (90 wt. %)	Graphite (10 wt. %)
3	$MgSO_4.7H_2O$ (80 wt. %)	Graphite (20 wt. %)
4	$MgSO_4.7H_2O$ (70 wt. %)	Graphite (30 wt. %)
5	$MgSO_4.7H_2O$ (90 wt. %)	Sugarcane bagasse (10 wt. %)
6	$MgSO_4.7H_2O$ (80 wt. %)	Sugarcane bagasse (20 wt. %)
7	$MgSO_4.7H_2O$ (70 wt. %)	Sugarcane bagasse (30 wt. %)
8	$NiSO_4.6H_2O$ (70 wt.%)	Graphite (30 wt.%)
9	$NiSO_4.6H_2O$ (70 wt. %)	Sugarcane Bagasse (30 wt.%)

3.5. Kinetic Study

The Vachusca and Voboril(43) and Speyer(46) model is a kinetic approach used to analyze thermal decomposition reactions by fitting TGA data with a sigmoid function. This function captures the characteristic S-shaped decomposition curve, allowing for a smooth and precise representation of mass loss over time. By applying this mathematical approach, the model enables the determination of key kinetic parameters such as activation energy (Ea.), reaction order (n), and coefficient of determination (R^2), which are essential for understanding the thermal stability and degradation mechanisms of materials.

A fundamental aspect of this model is that it uses the Arrhenius equation to explain how the reaction rate varies with temperature. The model transforms the decomposition data into a linear equation, where reaction order and activation energy can be extracted from the slope and intercept of a plotted function. This approach simplifies complex thermal degradation processes, making it easier to compare different materials and evaluate their kinetic behavior under controlled heating conditions.

One of the key advantages of the model is its ability to linearize TGA data, reducing errors associated with traditional nonlinear fitting methods. However, its accuracy depends on the quality of the sigmoid function fit and the assumption that decomposition follows a single-step reaction mechanism. Despite these limitations, the

Vachuska and Voboril and Speyer model remains a valuable tool in thermal analysis, particularly for materials where precise kinetic parameter estimation is necessary for process optimization and stability assessment.

To apply the Vachuska and Voboril and Speyer model to the obtained TGA data, we start by fitting the experimental data with a sigmoid function, capturing the typical S-shaped curve that represents the decomposition process. Once the sigmoid curve is fitted, we proceed with estimating the kinetic parameters such as activation energy (Ea), coefficient of determination (R^2), and reaction order (n). These parameters are essential for understanding the material's thermal stability and how the reaction progresses with temperature. The objective function used in the Vachuska and Voboril model is typically based on the least square method, which minimizes the difference between experimental and predicted values, helping to determine the optimal kinetic parameters. This step-by-step approach allows for a comprehensive analysis of the TGA data, providing valuable insights into the decomposition kinetics.

The Decomposition Rate:

The rate of decomposition, or mass loss, of a reactant in TGA is typically described by the equation 2.(49)

$$\frac{\mathrm{dm}}{\mathrm{dt}} = -\mathrm{km}^{\mathrm{n}} \qquad (2)$$

Where, m represents the reactant mass, k the reaction rate constant, n global reaction order and t an instant in time. During TG analysis, sample mass loss is measured as a function of time. Sample mass (X) and mass loss are related according to Equation 3:(43)

$$m = m_0 - m_0 \frac{w}{w_\infty} \qquad (3)$$

Where m_0 represents sample initial mass, w the mass loss at a given time, and w_∞ is the maximum mass loss associated with the thermal event of interest. After some algebraic manipulation, it is possible to calculate the first-time derivative of conversion (f) according to Equation 4.(50)

$$\frac{\mathrm{df}}{\mathrm{dt}} = \mathrm{km_0}^{\,\mathrm{n-1}}.(1-\mathrm{f})^{\mathrm{n}} \qquad (4)$$

To apply Equation 4 to experimental TG data, f must be calculated based on mass loss, which can be performed as described by Equation 5. (46)

$$f = \frac{\mathrm{w}}{\mathrm{w}^{\infty}} \qquad (5)$$

The reaction rate constant k depends on temperature following the Arrhenius law in (Equation 6)**,** where k_0 represents the Arrhenius pre-exponential factor, R the universal gas constant, T temperature and E_a process global activation energy.(46)

$$\mathrm{k} = \mathrm{k_0}.\,\mathrm{e}^{-\left(\mathrm{E_a}/\mathrm{RT}\right)} \qquad (6)$$

Through inserting Equation 6 into equation 4 and taking the natural logarithm of both sides, it is possible to arrive at Equation 7.(43)

$$ln\,\frac{df}{dt} = ln\left[k_0 m_0{}^{\,n-1}\right] + n\ln(1-f)^n \; - \frac{E_a}{RT} \qquad (7)$$

Next, taking the time derivative of Equation 7 and considering that temperature can be related with time and imposed heating rate (φ) according to Equation 8, the final equation to be applied to the measured TG data can be constructed Equation 9.(50)

$$T = T_r + \varphi t \quad (8)$$

$$(T_r + \varphi t)^2 \; \frac{{}^{d^2 f}\!/_{dt^2}}{{}^{df}\!/_{dt}} = -n\left[\frac{(T_r+\varphi t)^2\left(\frac{\mathrm{df}}{dt}\right)}{1-f}\right] + \frac{E_a \varphi}{RT} \quad (9)$$

Where, T_r represents a reference temperature, usually considered as the sample initial temperature, before heating is activated and $\frac{{}^{d^2 f}\!/_{dt^2}}{{}^{df}\!/_{dt}}$. can be calculated from the thermogravimetric curve and its derivatives. However, in order to apply Equation 9 to TG data, first, a sigmoid function for expressing the time dependence of conversion must be constructed (Equation 10)(49), so that the time derivatives of f involved in Equation 9 can be analytically evaluated.

$$f \; = \frac{1}{1+\exp\left(-\alpha.(t-\beta)\right)} \qquad (10)$$

The adjustable parameters α and β in Equation 10 must be estimated based on the experimental conversion values inside the time interval, where the thermal event is developing. n order to accomplish this task, a code based in the simplex algorithm(51) was constructed, which minimizes the deviations between experimental and calculated (Equation 10) conversion values, through a simultaneous variation of α and β.

Finally, based on Equation 9, two auxiliary variables can be introduced in the model (X and Y), given by Equations 11 and 12)(49), and with them, a linear function can be constructed (Equation 13)(43).

$$Y = (T_r + \varphi t)^2 \frac{d^2f/dt^2}{df/dt} = -n + \frac{E_a\varphi}{RT} \quad (11)$$

$$X = \left[\frac{(T_r + \varphi t)^2\left(\frac{df}{dt}\right)}{1-f}\right] \quad (12)$$

$$Y = -nX + \frac{E_a\varphi}{RT} \quad (13)$$

Through use of Equation 13, a plot of Y as a function of X can be used to evaluate process global activation energy and order through linear and angular coefficients, respectively.

4 Result and Discussion

4.1. Characterization

The table 3 shows the proximate analysis of Graphite and Sugarcane Bagasse, highlighting differences in moisture, volatile matter, and ash content. Graphite has extremely low moisture (0.1%) and volatile matter (0.1%), making it highly stable and non-reactive, with a very high fix carbon content (99.8%), indicating its purity as carbon.(52) Sugarcane Bagasse has significantly higher moisture (6.6%) and volatile content (87.6%) compared to literature. (47), making it highly combustible, with moderate fix carbon content (5.8%), which affects combustion efficiency.

Table 3. Proximate analysis of Graphite and Sugarcane Bagasse

Species	Moisture	Volatile	Fix carbon
Graphite	0.1	0.1	99.8
Sugarcane Bagasse	6.6	87.6	5.8

4.2. Thermodynamics Simulations

4.2.1 Magnesium sulfate thermal behavior

4.2.1.1. Dehydration Processes

Figure 2a illustrates the equilibrium states of magnesium sulfate hydrates as a function of temperature, but contrary to a strictly stepwise dehydration process, multiple hydration states coexist at given temperatures. Even at 25°C, the system contains a mixture of $MgSO_4 \cdot 7H_2O$, $MgSO_4 \cdot 6H_2O$, and $MgSO_4 \cdot 5H_2O$ rather than transitioning from one phase to another in a sequential manner. Around 50°C, for example, equilibrium exists between $MgSO_4 \cdot 7H_2O$, $MgSO_4 \cdot 6H_2O$, $MgSO_4 \cdot 5H_2O$, and $MgSO_4 \cdot 4H_2O$, demonstrating that different hydrates can be present simultaneously rather than forming one after the other. As the temperature increases, the equilibrium gradually shifts toward lower hydration states, with $MgSO_4 \cdot 4H_2O$ and $MgSO_4 \cdot H_2O$ dominating before the final transition to anhydrous $MgSO_4$ beyond 300°C. However, the interpretation that one sulfate phase with lower water content directly forms after another is inaccurate, as the equilibrium diagrams suggest that various hydrates coexist rather than following a linear dehydration sequence.

Figure 2b provides insights into the equilibrium speciation of gaseous products during thermal decomposition. At low temperatures, the gas phase is primarily composed of N_2, while water vapor concentration increases with progressive dehydration until approximately 140°C, when $MgSO_4 \cdot H_2O$ formation stabilizes the system. The water concentration remains nearly constant until 100°C, corresponding to the stability range of $MgSO_4 \cdot H_2O$, followed by a slight increase due to the transition to anhydrous $MgSO_4$. A significant transition occurs at approximately 80°C, where the decomposition of $MgSO_4$ initiates, producing SO_2, SO_3, and O_2, as shown in Equation 14. These gaseous products dilute the water vapor concentration, demonstrating that the presence and concentration of these gases are directly linked to the dehydration and decomposition stages of magnesium sulfate.

$$SO_3 = SO_2 + 0.5O_2 \qquad (14)$$

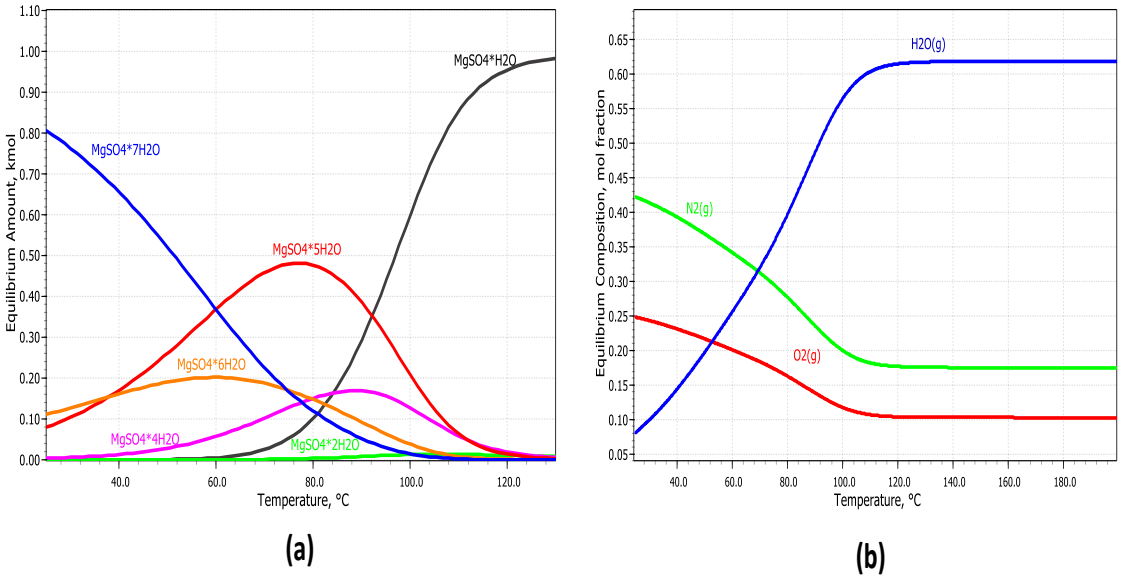

Figure 2. Equilibrium composition of the thermal decomposition of the $MgSO_4.7H_2O$ as a function of temperature. (a) Solid Phases of dehydration (b) Gas Phases of dehydration

4.2.1.2. Desulfation Process

The decomposition of anhydrous $MgSO_4$ initiates at approximately 600°C, marking the onset of desulfation, as illustrated in Figure 3a. Initially, $MgSO_4 \cdot H_2O$ dehydrates completely around 300°C, forming anhydrous $MgSO_4$.

Beyond 600°C, $MgSO_4$ begins to decompose, yielding MgO as the final solid residue is shown in equation 15. At 700-800°C, the equilibrium concentration of $MgSO_4$ reaches a peak due to a balance between its formation and decomposition rates. However, at temperatures exceeding 800°C, the decomposition process accelerates, leading to the complete disappearance of $MgSO_4$ above 1100°C.

$$MgSO_4 = MgO + SO_2 + 0.5O_2 \qquad (15)$$

As temperature increases beyond 600°C, sulfur-containing gases (SO_2 and SO_3) begin to form, with SO_2 being the dominant species at high temperatures. The equilibrium diagram (Figure 3b) reveals that SO_3 is present in minor quantities, suggesting that most sulfur is released as SO_2. Additionally, O_2 evolution is observed above 800°C, confirming an oxidative environment that drives sulfate breakdown. The final gas composition mainly consists of SO_2 and O_2, with SO_3 levels decreasing at extreme temperatures due to thermal decomposition.

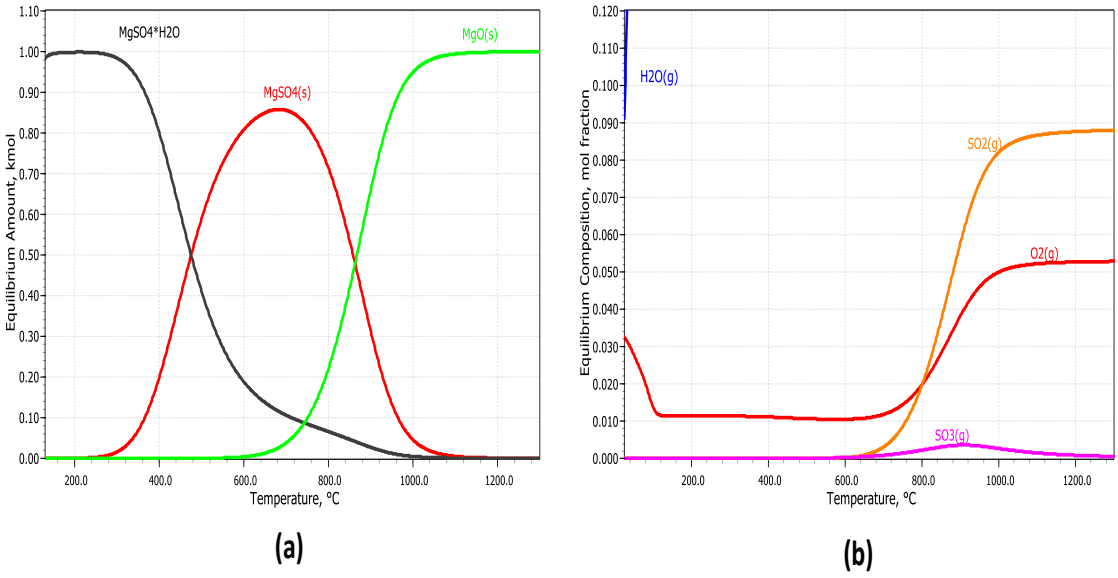

Figure 3. Equilibrium composition of the thermal decomposition of the $MgSO_4.7H_2O$ as a function of temperature. (a) Solid Phases of desulfation (b) Gas Phases of desulfation

4.2.2. Magnesium Sulfate under the presence of Graphite

4.2.2.1. Dehydration Processes

In the solid-phase behavior, the thermal decomposition of the mixture containing 70% $MgSO_4 \cdot 7H_2O$ and 30% carbon (graphite) shows that magnesium sulfate hydrates undergo a progressive dehydration as the temperature rises. Initially, $MgSO_4 \cdot 7H_2O$ begins to dehydrate around 30 °C, and through successive stages, intermediate hydrates such as $MgSO_4 \cdot 6H_2O$, $MgSO_4 \cdot 4H_2O$, $MgSO_4 \cdot 2H_2O$, and $MgSO_4 \cdot H_2O$ appear and disappear between approximately 30–110 °C. After around 90 °C, the anhydrous form of $MgSO_4$ dominates and remains stable above 120 °C. Graphite, shown as a constant horizontal line, remains in the system throughout the process, indicating it does not sublimate, even at temperatures well below its sublimation point (~3600 °C). This highlights that graphite, rather than being a passive participant, is chemically involved in the process. It actively participates in the redox reactions, interacting with intermediate species such as SO_3, O_2, and $MgSO_4$. This confirms graphite's role as a solid-phase reductant, contributing significantly to the reaction even at relatively low temperatures, below 150 °C.

The possible effects of carbon-bearing materials, particularly graphite, on the overall reaction mechanism is crucial. Graphite interacts with sulfate species in both their monohydrated (e.g., $MgSO_4 \cdot H_2O$) and anhydrous (e.g., $MgSO_4$) forms, significantly influencing the decomposition process. In particular, the interaction between CO and these sulfate species can lead to the reduction of magnesium sulfate and the formation of other by-products such as CO_2 or magnesium oxide MgO. Graphite is not simply a passive material in the system, but actively participates in redox reactions with sulfate species, driving the transformation of the material in ways that would not occur in its absence. This active role of graphite provides valuable insights into the reaction pathways and product formation, indicating that graphite's interaction with sulfate species can modify the overall decomposition mechanism, influencing both the rate and nature of the transformation.

In the gas-phase behavior, water vapor (H_2O) evolves rapidly after 40 °C, reaching a plateau at around 110 °C, indicating the completion of the

dehydration process. As the temperature rises, oxygen (O_2) concentration declines, suggesting that it is involved in redox reactions. Notably, CO_2 begins to appear around 80 °C, with a slight increase up to 130 °C, which signals the partial oxidation of graphite. Despite graphite's high sublimation temperature, it reacts with oxygen species and magnesium sulfate, undergoing oxidation to form CO and CO_2. This demonstrates that graphite is chemically consumed in the process, actively contributing to the reduction of species like O_2 and SO_3. Thermodynamically, this confirms that graphite is an effective reductant, facilitating redox reactions and CO_2 generation even at low temperatures, which would otherwise not be expected due to its high sublimation point. This active involvement of graphite in the redox processes emphasizes its role in modifying the decomposition mechanism of magnesium sulfate and influencing the overall thermal reaction.

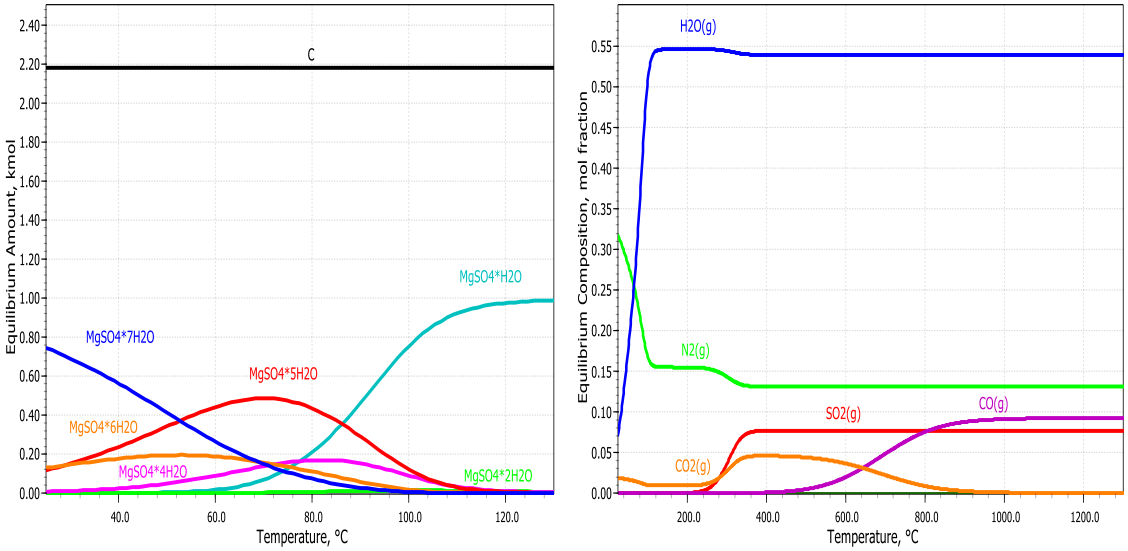

Figure 4. Equilibrium composition of the thermal decomposition of the 70%$MgSO_4.7H_2O$ mixed with 30%Carbon as a function of temperature. (a) Solid Phases of dehydration (b) Gas Phases of dehydration

4.2.2.2. desulfation Process

At temperatures (~600°C), the anhydrous $MgSO_4$ begins decomposing, marking the onset of desulfation is shown in figure 5. However, the interaction with graphite follows a distinct pathway compared to conventional gas-solid reduction. The

speciation diagram allows for a more precise evaluation of this temperature range, confirming that the decomposition initiates at approximately 600°C. Unlike a purely thermally driven breakdown, a solid-solid interaction between sulfate and graphite appears to play a direct role in the reaction. This interaction leads to the simultaneous formation of CO_2 and SO_2, suggesting a direct reaction between $MgSO_4$ and graphite. Notably, CO formation is only observed after complete MgO production, implying that it results from the subsequent interaction of O_2 with residual graphite rather than from the initial sulfate reduction.

To better describe this process, the following global reaction equation should be introduced:

$$\mathrm{MgSO_4} + C = MgO + SO_2 + C0_2 \qquad (16)$$

This reaction highlights the direct role of graphite in facilitating sulfate reduction. The observed trends in CO and CO_2 formation further support this mechanism, emphasizing that CO is only produced after MgO formation.

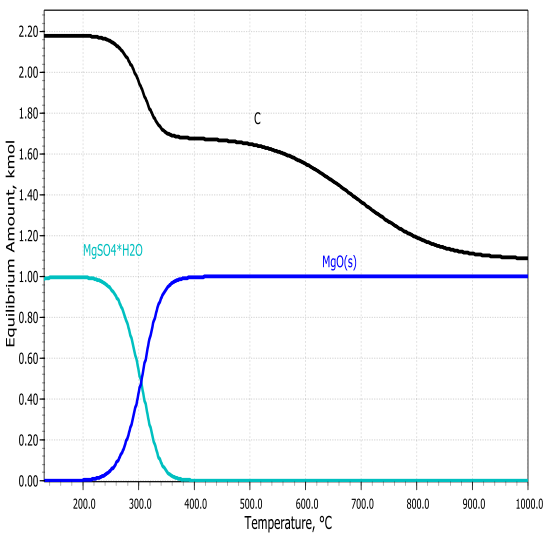

(a)

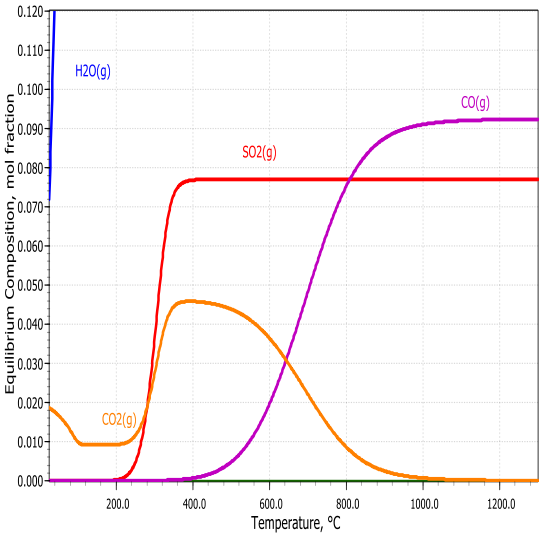

(b)

Figure 5. Equilibrium composition of the thermal decomposition of the 70%MgSO4.7H2O mixed with 30%Carbon as a function of temperature. (a) Solid Phases of desulfation (b) Gas Phases of desulfation

4.2.3. Magnesium Sulfate under the presence of Graphite with inert atmosphere

The effect of graphite addition on the thermochemical tendencies discussed so far can be inferred from Figure 6a, which presents equilibrium data for an initial solid mixture containing 10% (w/w) of graphite. It is evident from the figure that while the presence of the reducing agent does not influence the dehydration processes, it significantly impacts the thermal decomposition of the anhydrous magnesium sulfate ($MgSO_4$). This influence manifests as a substantial driving force for the decomposition reaction, as reflected by the markedly lower equilibrium mass fraction of $MgSO_4$ compared to the behavior depicted in Figure 2a. Furthermore, the maximum equilibrium mass fraction of $MgSO_4$ is shifted to a much lower temperature, approximately 340°C.

The pronounced effect of graphite can be understood through its chemical reaction with oxygen (O_2) formed during the thermal decomposition of $MgSO_4$. This reaction consumes O_2, effectively shifting the decomposition equilibrium towards the formation of magnesium oxide (MgO). As a result, $MgSO_4$ decomposition is completed at a significantly lower temperature, around 400°C, compared to the case without graphite, where MgO mass fraction reaches a maximum only after 1100°C. This equilibrium shift also enhances the driving force for the dehydration of $MgSO_4.H_2O$, which is completed by approximately 400°C in the presence of graphite.

The behavior of graphite at higher temperatures further illustrates its role in the system. After approximately 600°C, the reduction in graphite mass fraction is attributed to the Boudouard reaction ($C + CO_2 \rightarrow 2CO$), which leads to the formation of carbon monoxide (CO). As MgO and graphite become the sole solid phases in the system, the mass fraction of magnesium oxide increases while that of graphite decreases. This progression highlights the interplay between the reducing agent and the thermal decomposition processes.

Another notable observation from Figure 6b is the absence of sulfur trioxide (SO_3) in the equilibrium gas-phase composition. This suggests that the presence of graphite also shifts the equilibrium for SO_3 decomposition ($SO_3 \rightarrow SO_2 + O_2$) by consuming the oxygen produced during the reaction. This additional shift underscores the role of the reducing agent in altering the thermodynamic pathways of the system. Interestingly, increasing the graphite mass fraction does not fundamentally change the thermochemical tendencies observed in Figure 2. The variations in the mass fractions of solid phases and the concentrations of gaseous species are solely related to the changes in the initial masses of $MgSO_4$ and the reducing agent. This indicates that the thermochemical behavior of the system is primarily governed by the interaction between the sulfate and the reducing agent, rather than the absolute quantities of the reactants.

The addition of graphite introduces significant modifications to the thermal decomposition pathways of magnesium sulfate. By facilitating oxygen consumption and altering equilibrium conditions, graphite not only lowers the decomposition temperature of $MgSO_4$ but also accelerates the overall reaction progression. These findings have important implications for processes that rely on reducing agents to enhance thermal stability and decomposition efficiency in sulfate-based systems.

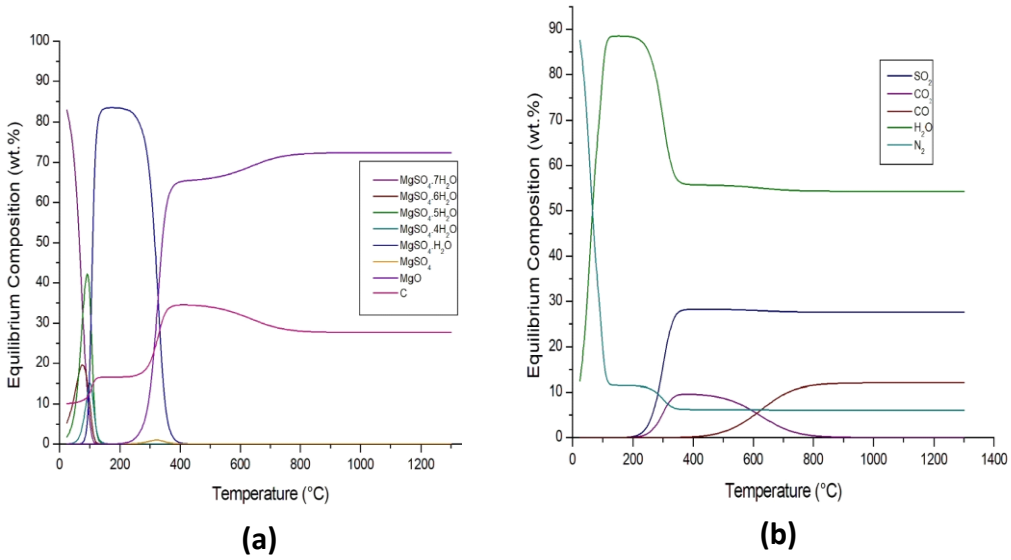

Figure 6. Equilibrium composition of the thermal decomposition of the 90%MgSO4.7H2O mixed with 30%Carbon as a function of temperature. (a) Solid Phases; (b) Gas Phases

4.2.4. Nickel sulfate thermal behavior

4.2.4.1 Dehydration Processes

Figure 7 illustrates the equilibrium states of nickel sulfate hydrates as a function of temperature, highlighting the stepwise dehydration process. At 25°C, $NiSO_4 \cdot 6H_2O$ is the stable phase, but as the temperature increases, the first crystallization water is lost, forming $NiSO_4 \cdot 4H_2O$ around 100°C. This transformation continues as $NiSO_4 \cdot 4H_2O$ dehydrates into $NiSO_4 \cdot H_2O$ near 150°C. The anhydrous $NiSO_4$ phase appears beyond 300°C, signifying the complete loss of hydration water. A more quantitative comparison is necessary to substantiate claims regarding the relative simplicity of nickel sulfate dehydration. The critical point here is that nickel sulfate dehydration follows a stepwise mechanism, and while it appears to occur within a narrower temperature range than magnesium sulfate, this must be explicitly quantified for clarity.

Figure 7b provides insights into the equilibrium speciation of gaseous products during nickel sulfate thermal decomposition. At lower temperatures, $H_2O(g)$ is dominant, corresponding to the progressive dehydration steps. However, the

statement that water vapor concentration decreases beyond 100°C due to the stabilization of $NiSO_4 \cdot H_2O$ is incorrect. In reality, the water mole fraction only decreases significantly after the onset of thermal decomposition, when O_2 formation becomes significant, typically around 200°C. Additionally, the claim that nickel sulfate releases higher amounts of SO_3(g) than magnesium sulfate is not well-supported. Without a quantitative comparison, this statement remains vague, as the equilibrium data suggest that SO_3 amounts in both systems are quite similar. Furthermore, while nickel monohydrate does decompose at a lower temperature range than magnesium monohydrate, the difference in decomposition temperatures between the anhydrous sulfates is not as pronounced.

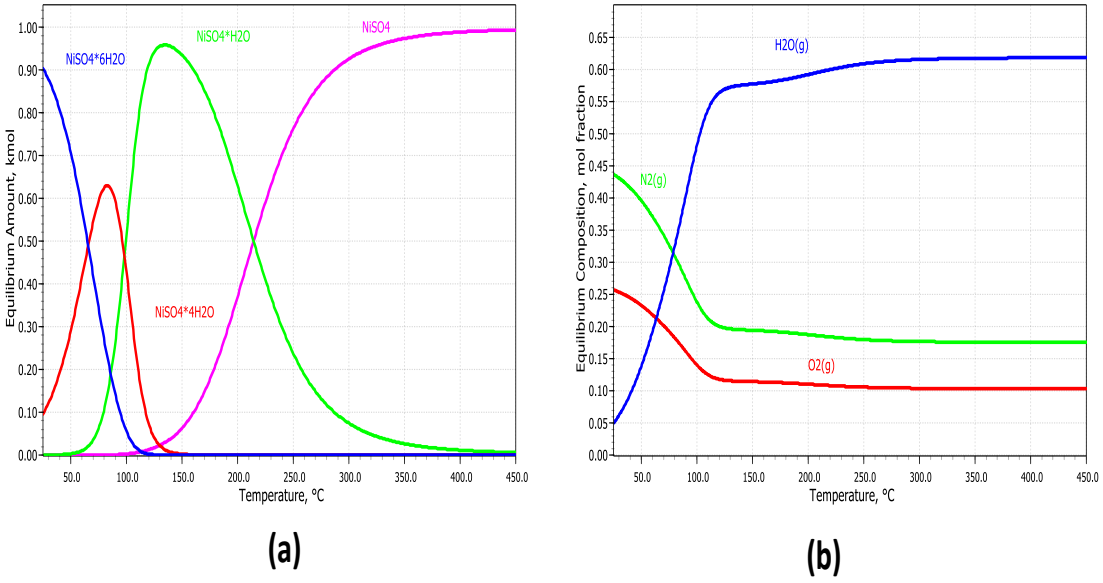

Figure 7. Equilibrium composition of the thermal decomposition of the $NiSO_4.6H_2O$ as a function of temperature. (a) Solid Phases of dehydration (b) Gas Phases of dehydration

4.2.4.2. Desulfation Process

The decomposition of anhydrous $NiSO_4$ initiates at around 700°C, marking the onset of desulfation, as displayed in Figure 8. As temperature increases, $NiSO_4$ progressively breaks down into NiO while releasing sulfur-containing gaseous species, primarily SO_2 and SO_3 is displayed in equation 17. However, the claim that $NiSO_4$ remains stable over a broader range compared to $MgSO_4$ is incorrect. $NiSO_4$

decomposes at a lower temperature range than $MgSO_4$, indicating that it is less thermally stable. This contradicts the assertion that nickel sulfate has stronger sulfate bonding; instead, it suggests that magnesium sulfate requires more energy for complete decomposition. Additionally, the predominant gaseous species in this process must be identified, particularly the role of O_2 formation as shown in equation 19, which has not been discussed.

$$NiSO_4 = NiO + SO_3 \qquad (17)$$

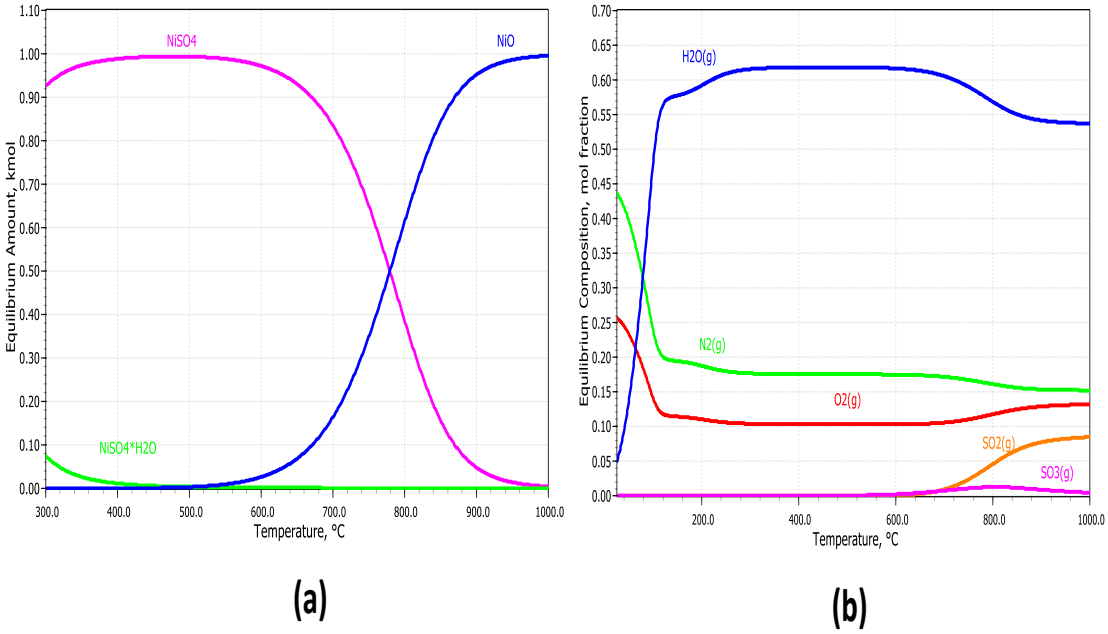

Figure 8. Equilibrium composition of the thermal decomposition of the $NiSO_4.6H_2O$ as a function of temperature. (a) Solid Phases of desulfation (b)gas phase of desulfation

4.2.5. Nickel sulfate under the presence Graphite

4.2.5.1 Dehydration and desulfation processes

In the solid-phase behavior, the equilibrium states of nickel sulfate hydrates in the presence of graphite, as shown in Figure 9a, reveal a stepwise dehydration process similar to the pure system. $NiSO_4 \cdot 6H_2O$ dehydrates to form $NiSO_4 \cdot 4H_2O$ (~80°C), $NiSO_4 \cdot 2H_2O$ (~120°C), and $NiSO_4 \cdot H_2O$ (~160°C) before reaching the anhydrous state above 250°C. However, unlike the pure system, the

presence of graphite causes $NiSO_4 \cdot H_2O$ and $NiSO_4$ to coexist over a wider temperature range, indicating a slower and more complex dehydration process. This suggests that the interaction of nickel sulfate with graphite influences its phase transitions, making its behavior distinct from other sulfates such as magnesium sulfate. Each sulfate exhibits a unique tendency to interact with graphite, emphasizing the need to analyze equilibrium phase composition trends individually.

A detailed examination of the impact of carbon-bearing materials, particularly graphite, on the overall reaction mechanism is crucial. In the case of nickel sulfate, which primarily exists in an anhydrous form at higher temperatures, graphite directly influences the redox reactions leading to CO and CO_2 formation. Graphite is not merely a passive material; it actively engages in redox reactions with sulfate species. Specifically, carbon (graphite) can reduce $NiSO_4$ to NiO, with the release of CO and SO_2, following a solid-solid reaction pathway. The direct reaction between graphite and sulfate species bypasses the need for thermal desulfation alone, allowing the reduction process to occur at significantly lower temperatures. This is evident as the formation of NiO starts around 200°C in the presence of graphite, compared to ~700°C in the absence of graphite. The interaction between CO, produced from graphite oxidation, and nickel sulfate further accelerates the reduction process.

In contrast to magnesium sulfate, where graphite's impact on desulfation is also observed but less pronounced, nickel sulfate is far more reactive in the presence of graphite. The direct solid-solid interaction between graphite and nickel sulfate facilitates the rapid conversion of $NiSO_4$ to NiO, coupled with the evolution of gaseous CO_2 and SO_2. This behavior underscores the catalytic role of graphite in promoting sulfate reduction, driven by the formation and reactivity of CO. To clarify the decomposition pathways, the following chemical reactions should be included:

$$NiSO_4 + C = NiO + SO_2 + C0_2 \qquad (18)$$

4.2.5.2. Gaseous Phase Evolution

Figure 9b presents the equilibrium gas-phase composition during nickel sulfate decomposition with graphite. Initially, $H_2O(g)$ dominates, peaking around 100°C, corresponding to dehydration stages. Unlike the pure system, $CO_2(g)$

appears early (~50°C) and increases continuously, suggesting a direct interaction between graphite and sulfate species. A key observation is the simultaneous presence of SO_2(g) and CO_2(g), reinforcing the idea that $NiSO_4$ directly reacts with graphite without requiring an intermediate CO step. This trend differs from magnesium sulfate, where CO formation is observed only after MgO is fully produced, indicating a different interaction pathway. The absence of CO below 300°C is expected due to the thermodynamic stability of CO_2 at these temperatures. Additionally, the earlier onset of SO_2 evolution suggests that nickel sulfate undergoes desulfation at lower temperatures compared to magnesium sulfate. It is important to note that in both cases, no SO_3 formation occurs because oxygen is consumed in the formation of CO_2 or CO, preventing SO_3 from forming via the reaction:

$$2CO_2 = 2CO + O_2 \qquad (19)$$

$$C + 0.5O_2 = CO \qquad (20)$$

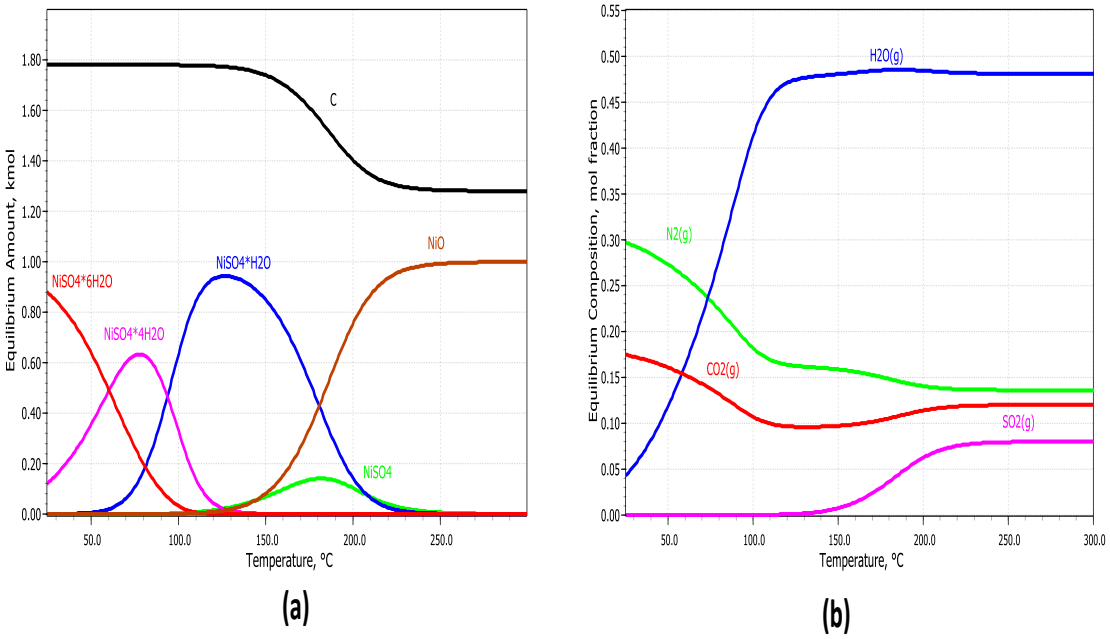

Figure 9. Equilibrium composition of the thermal decomposition of the 70%$NiSO_4.6H_2O$ with 30%Carbon as a function of temperature. (a) Solid Phases (b) Gas Phases

4.2.6. Nickel Sulfate under the presence of Graphite with inert atmosphere

The equilibrium compositions of the solid phases of the thermal decomposition of $NiSO_4 \cdot 6H_2O$ with carbon as a reducing agent are presented in Figure 10a. $NiSO_4 \cdot 6H_2O$ starts to dehydrate between 100°C and 200°C, resulting in $NiSO_4 \cdot 4H_2O$. The tetrahydrate phase further dehydrates into $NiSO_4 \cdot H_2O$ as the temperature rises to around 200–300°C. At approximately 300°C, the dehydration process concludes with the formation of anhydrous $NiSO_4$, which remains the dominant phase up to 600–700°C. At higher temperatures, carbon participates in the reduction of $NiSO_4$ to NiO. This reaction becomes significant above 600°C, and as the temperature continues to rise, NiO becomes the stable and prevailing solid phase beyond 800°C. The addition of carbon does not influence the dehydration temperatures of $NiSO_4$ hydrates but facilitates the reduction of $NiSO_4$ to NiO at elevated temperatures.

The gas-phase thermal decomposition of $NiSO_4 \cdot 6H_2O$ with carbon as a reducing agent is illustrated in Figure 10b. Below 300°C, water vapor (H_2O) is the primary gas released during the dehydration of $NiSO_4 \cdot 6H_2O$. Between 600°C and 800°C, the decomposition of $NiSO_4$ produces sulfur dioxide (SO_2) and carbon dioxide (CO_2) as the dominant gases due to the reaction between carbon and the sulfate. The addition of carbon prevents the formation of oxygen (O_2) and sulfur trioxide (SO_3) by actively reacting with the sulfate and promoting reduction processes. At temperatures above 800°C, the gas phase primarily consists of SO_2 and CO_2, marking the complete reduction of $NiSO_4$ to NiO. The absence of O_2 and SO_3 highlights the critical role of carbon in altering the gas-phase composition during thermal decomposition.

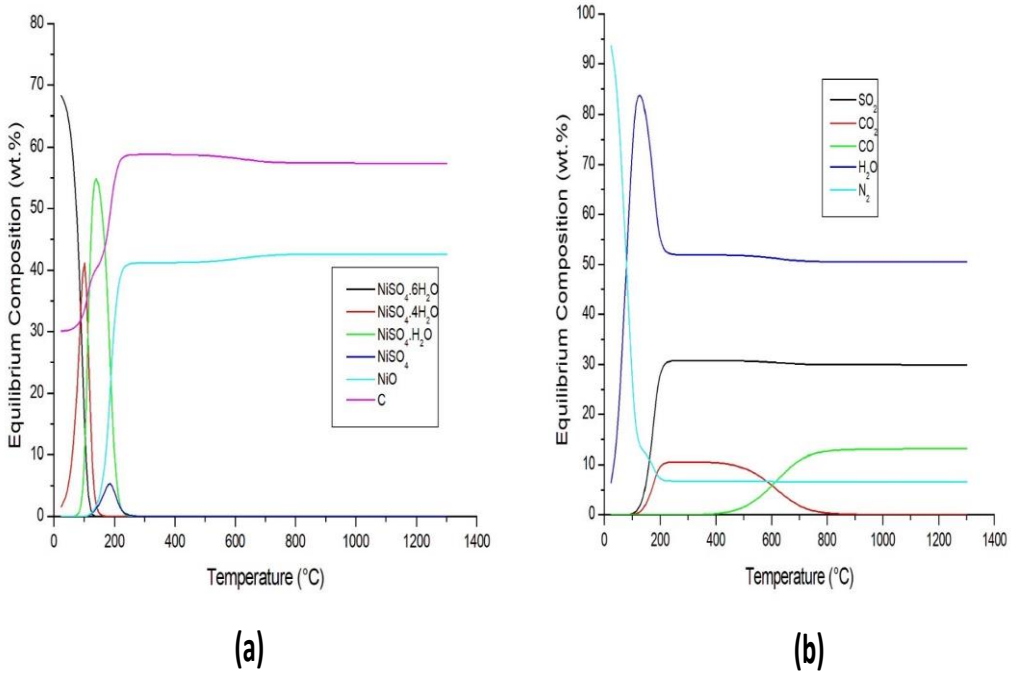

Figure 10. Equilibrium composition of the thermal decomposition of the 70%NiSO4.6H2O mixed with 30%Carbon as a function of temperature. (a) Solid Phases (b) Gas Phases

4.3. Thermogravimetric Analysis

4.3.1 Magnesium Sulfate thermal behavior

Figure 11a and 12a show the TGA and DTG curves for pure magnesium sulfate and its mixture with graphite and sugarcane bagasse, illustrating the distinct decomposition stages. All curves indicate significant mass loss below 300°C, primarily due to water desorption and dehydration, consistent with previous studies.(7,9)

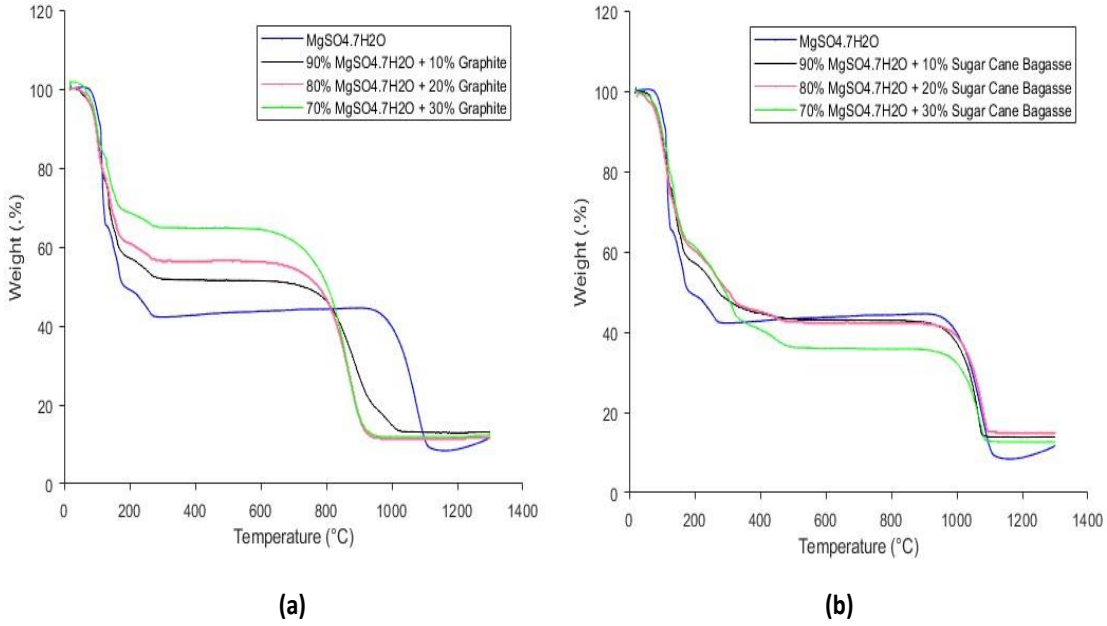

Figure 11. TGA measurements of the decomposition of 90,80,70%$MgSO_4.7H_2O$ (a) 10,20,30% graphite (b)10,20,30% Sugarcane Bagasse

Derivative thermogravimetry (DTG) curves of pure magnesium sulfate (Figure 12a) reveal a clear stepwise decomposition pattern, particularly during the dehydration process. Specifically, three distinct stages are observed. The first stage (100–120°C) is characterized by the loss of three water molecules, resulting in a 27.62% mass loss (calculated 27.2%). The second stage (120–190°C) shows a sharp DTG peak, indicating the release of two additional water molecules with an observed mass loss of 13.48% (calculated 13.2%). The third stage (190–280°C) corresponds to the loss of one water molecule, leading to a 6.30% weight reduction (calculated 6.8%). Beyond 280°C, the TGA and DTG curves remain stable, confirming the formation of anhydrous $MgSO_4$, which subsequently decomposes above 950°C with a sharp DTG

peak, indicating desulfation. This final stage is characterized by a 32.89% mass loss (calculated 30.26%) due to the release of SO_2 and O_2, forming MgO.

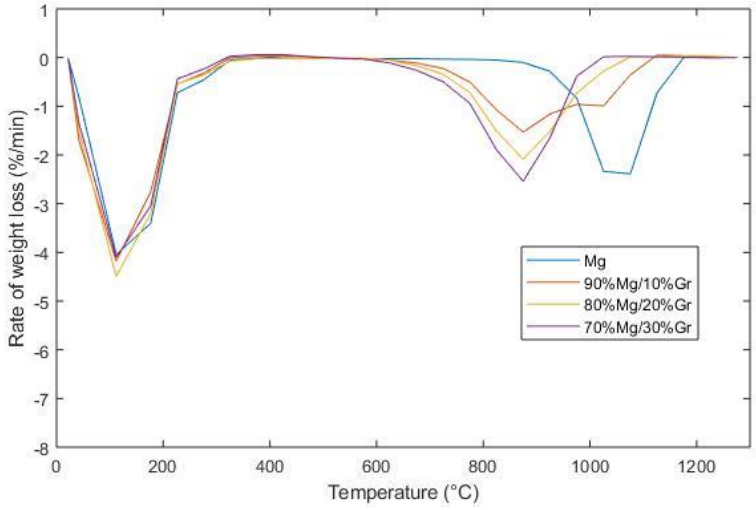

(a)

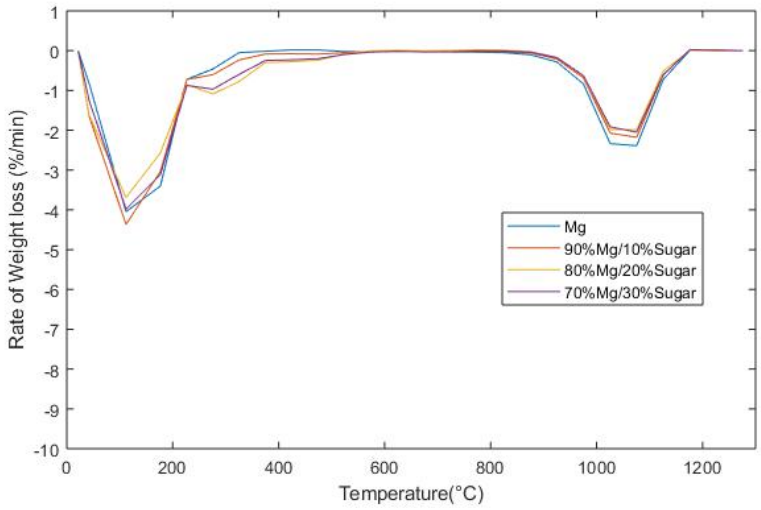

(b)

Figure 12 DTG measurements of the decomposition of 90,80,70%$MgSO_4.7H_2O$ (a) 10,20,30% graphite (b)10,20,30% Sugarcane Bagasse

This stepwise decomposition behavior aligns with the mechanism observed in nickel sulfate ($NiSO_4$), which also decomposes through multiple distinct stages. The similarity between the decomposition behaviors of $MgSO_4$ and $NiSO_4$ supports the hypothesis that such stepwise mechanisms may be a characteristic of metal sulfates in general. The experimental and calculated values of mass loss for each stage

closely match (total experimental loss of 80.29% versus a calculated value of 78.01%), further confirming the accuracy of the decomposition mechanism described. Similar results were reported by Wang et al.(35), who noted comparable decomposition behaviors in their study. The theoretical and experimental values for mass loss at different stages are presented in Table 4 and represented by following equations.

$$MgSO_4.7H_2O = MgSO_4.3H_2O + 4H_2O \quad (21)$$

$$MgSO_4.3H_2O = MgSO_4.H_2O + 3H_2O \quad (22)$$

$$MgSO_4.H_2O = MgSO_4 + H_2O \quad (23)$$

$$MgSO_4 = MgO + SO_3 \quad (24)$$

Table 4. The theoretical, experimental values of mass loss of pure magnesium sulfate

Reaction	Temperature (°C)	Mass Loss (%) Found	Mass Loss (%) Calculated
Equation 21	140	27.29	27.62
Equation 22	165.7	13.62	13.48
Equation 23	300.2	6.81	6.3
Equation 24	1050.7	30.26	32.89

The TGA and DTG analyses were also used to examine the effect of adding graphite to magnesium sulfate. The TGA curve confirms that dehydration remained unchanged, but the decomposition temperature shifted to lower values, aligning with thermodynamic simulations. The DTG curve provides further insight into the decomposition process, displaying distinct peaks corresponding to the mass loss steps observed in TGA. All sulfate mixtures underwent complete decomposition, with final mass losses exceeding 85%, as seen for pure $MgSO_4$. A stable endpoint was achieved in all cases, confirming the completion of sulfate decomposition. The theoretical and experimental values of mass loss are presented in Table 5.

Table 5. Calculated and experimental mass loss of (a) 90% $MgSO_4.7H_2O$ +10%Graphite (b) 80% $MgSO_4.7H_2O$ +20%Graphite (c) 70% $MgSO_4.7H_2O$ +30%Graphite

Reaction	**Temperature**	**(a)Theoretical weight loss (%)**	**(b)Theoretical weight loss (%)**	**(c)Theoretical weight loss (%)**
Equation 22	151.8	18.51	17.09	16.59
Equation 23	169.0	6.17	5.69	5.53
Equation 24	950.7	36.80	41.65	43.30

According to Miao et al. (53) and Tao et al. (54), expanded graphite (EG) lowers the onset decomposition temperature, which is evident from the TG and DTG curves shifting toward lower values. This effect is attributed by the authors to graphite's high thermal conductivity, which enhances heat transfer and accelerates sulfate decomposition. The DTG peaks reveal that the decomposition of anhydrous $MgSO_4$ occurs starts at 900°C in graphite-containing samples, compared to 1050°C in pure $MgSO_4$, confirming the effect of carbon, already reported based on thermodynamic simulations. The TGA results under inert atmosphere from e Souza et al(45) showed that $MgSO_4 \cdot 7H_2O$ undergoes stepwise dehydration between 30–150°C, followed by decomposition of $MgSO_4$ above 500°C. The presence of carbon-based reducing agents altered the decomposition pathway, Interestingly, the 90/10 $MgSO_4$/graphite mixture exhibited a slightly higher decomposition temperature than other mixtures, likely due to a lower availability of excess carbon, which limited the extent of reduction and heat transfer effects.

The TGA and DTG analyses of magnesium sulfate and sugarcane bagasse mixtures (Figure 11b, 12b) reveal that the decomposition temperature of $MgSO_4 \cdot 7H_2O$ remains unaffected by the presence of bagasse. Sugarcane bagasse, a lignocellulosic material, is composed primarily of cellulose (32–48%), hemicellulose (23–32%), lignin (19–24%), and ash (1.5–5%) .(38) The TGA curve shows that the initial weight loss at 300°C for the bagasse mixture is similar to pure $MgSO_4 \cdot 7H_2O$, indicating that bagasse does not significantly influence sulfate dehydration. . As the bagasse content increases, the residual weight decreases, suggesting that the amount of volatile oxidized products

such CO or CO_2 gets higher. These molecules could be formed through reaction with available O_2, which was continuously injected together with N_2 during TGA analysis. Silva et al. (55) observed similar results in their study of titanium dioxide–sugarcane bagasse mixtures, reinforcing the consistency of the observed decomposition behavior. Bruno et al(25) investigated the carbothermic reduction of magnesium sulfate heptahydrate ($MgSO_4 \cdot 7H_2O$) to synthesize highly reactive magnesium oxide (MgO) powder. This process involves heating $MgSO_4 \cdot 7H_2O$ in the presence of a carbon source, such as graphite, under a reducing atmosphere. The study found that the carbothermic reduction of $MgSO_4 \cdot 7H_2O$ could produce MgO at temperatures around 800°C, which is significantly lower than the temperatures typically required for the direct carbothermic reduction of MgO. This reduction in temperature is advantageous as it leads to the formation of MgO with distinct characteristics, including higher reactivity and smaller particle size. The TGA results under inert atmosphere from Souza et al(45) showed that $MgSO_4 \cdot 7H_2O$ undergoes stepwise dehydration between 30–150°C, followed by decomposition of $MgSO_4$ above 500°C. The presence of carbon-based reducing agents altered the decomposition pathway,

The TGA and DTG provide valuable insights into the thermal decomposition of pure graphite and sugarcane bagasse, as shown in Figure 13. The TGA curve for graphite remains nearly stable up to 600°C, which is typical for carbon materials that are resistant to thermal degradation at lower temperatures. However, a significant mass loss of approximately 8–10% occurs between 600°C and 700°C, likely due to oxidation.(52) This behavior is crucial to investigate, as it corresponds to the temperature range where gaseous molecules, including valuable reducing agents such as CO, begin to form.

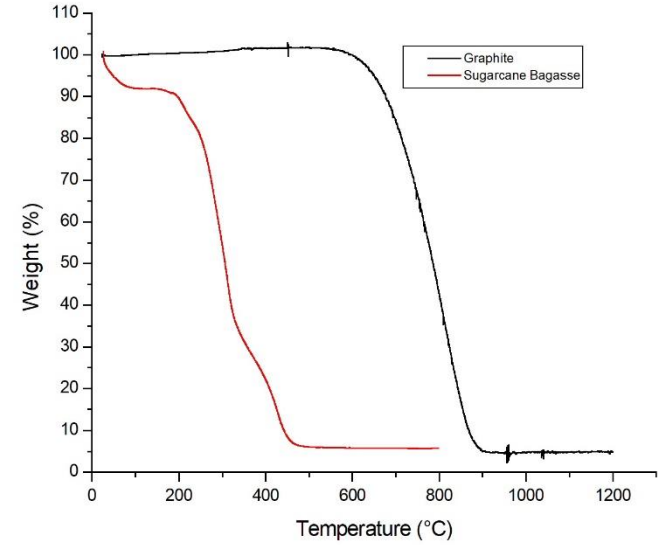

(a)

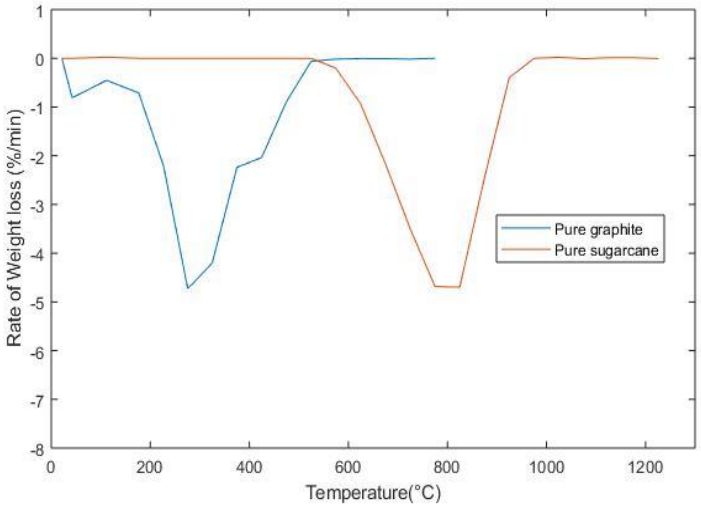

(b)

Figure 13. TGA and DTG measurements of the decomposition of pure graphite and pure Sugarcane Bagasse

The TGA and DTG curves for sugarcane bagasse reveal its multi-stage thermal behavior in an oxidative atmosphere. Initially, a minor mass loss (~8–12%) occurs below 150°C, attributed to the evaporation of moisture. The major decomposition phase starts around 200°C and extends up to 600°C, primarily driven by the oxidation of biomass components. Hemicellulose decomposes first (200–300°C), followed by cellulose degradation (300–400°C), which is evident from the

broad DTG peak around 300°C. Lignin, a more thermally stable component, decomposes over a broader range (400–600°C), contributing to a second distinct DTG peak near 500°C. In an oxidative environment, these reactions are accompanied by combustion, leading to the formation of CO_2, CO, and other volatile organic compounds. The total mass loss reaches approximately 85–90%, leaving minimal solid residue. Other researchers have also observed similar behavior. (56,57,58)

4.3.2. Nickel Sulfate thermal behavior

Figure 14 and 15 show the TGA and DTG curves of the test conducted with nickel sulfate with mixture of graphite and sugarcane bagasse. In pure nickel sulfate the TGA curve indicates that water loss begins at approximately 140°C, corresponding to the loss of two water molecules. This is supported by the mass loss data, where the found value is 14.5%, closely matching the calculated value of 13.7%. Tomaszewicz et al(19) reported an initial mass loss of 13.9%, while Straszko et al. (20) observed 14.2%, showing a strong agreement with our findings. Between 140°C and 300°C, an additional mass loss occurs due to the simultaneous evolution of three water molecules, with an observed mass loss of 21.22% (calculated 20.56%). This is consistent with the findings of Tomaszewicz and Kotfica (19), who reported a mass loss of 21.0%, and Straszko et al. (20), who observed 20.8%. The progressive loss of water molecules in this range indicates the gradual formation of the anhydrous sulfate phase. The final stage of dehydration occurs between 300°C and 380°C, where the removal of the last water molecule results in a mass loss of 7.3% (calculated 6.85%). This value aligns well with the reported mass losses of 7.1% and 7.4% from references(19)(20), respectively. At temperature 190 °C, the DTG curve shows a steep decline, ending around 820°C, with a found mass loss of 29.7% (calculated 30.45%). This significant mass loss corresponds to the decomposition of the anhydrous compound and the formation of the stable NiO phase presenting by equation 28. Tomaszewicz et al(19) and Straszko et al. (20)reported final mass losses of 30.1% and 29.5%, respectively, which closely match our findings. The theoretical and experimental values are summarized in Table 6.

$$NiSO_4.6H_2O = NiSO_4.4H_2O + 2H_2O \quad (25)$$

$$NiSO_4.4H_2O = NiSO_4.H_2O + 3H_2O \quad (26)$$

$$NiSO_4.H_2O = NiSO_4 + H_2O \quad (27)$$

$$NiSO_4 = NiO + SO_3 \quad (28)$$

Table 6. Theoretical and experimental values of mass loss of pure nickel sulfate.

Reaction	Temperature (°C)	Mass Loss (%) Found	Mass Loss(%) Calculated
Equation 25	139.9	14.5	13.7
Equation 26	300.1	21.22	20.56
Equation 27	380.9	7.3	6.85
Equation 28	812.8	29.7	30.45

The TGA curve in Figure 14 of the 70% $NiSO_4$ and 30% graphite mixture exhibits distinct mass loss stages, influenced by both dehydration and reduction processes. The first DTG peak indicates that graphite, and particularly sugarcane bagasse (SB), affect the dehydration behavior of the sample. The presence of SB introduces additional thermal events, which are likely associated with the oxidation of biopolymers such as cellulose, hemicellulose, and lignin. These organic components interact with oxygen released during decomposition, contributing to the observed weight losses, and modifying the thermal profile of the mixture. Initially, water loss begins at 180°C, corresponding to the removal of two water molecules. Between 180°C and 420°C, additional water molecules are gradually released, leading to the formation of anhydrous $NiSO_4$. The DTG in figure 15 curve highlights these dehydration steps as well-defined peaks, confirming the sequential nature of water loss.

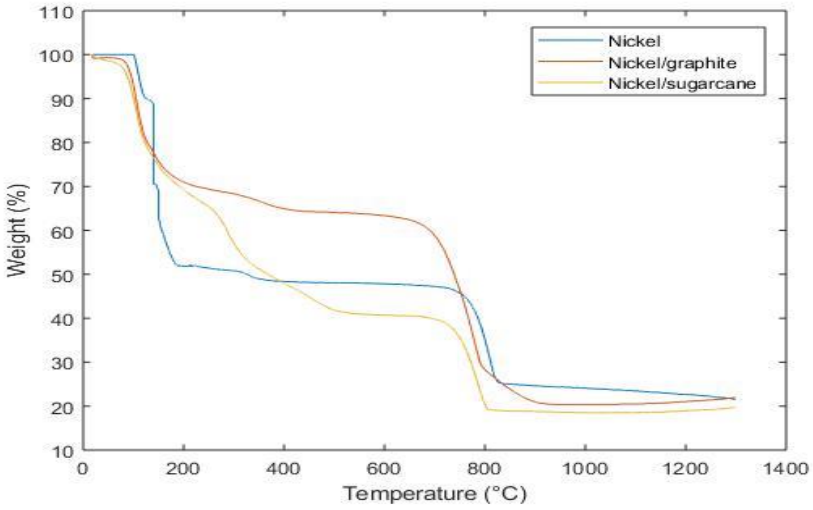

Figure 14. TGA measurements of the decomposition of NiSO4.6H2O with 30%graphite and 30% Sugarcane Bagasse

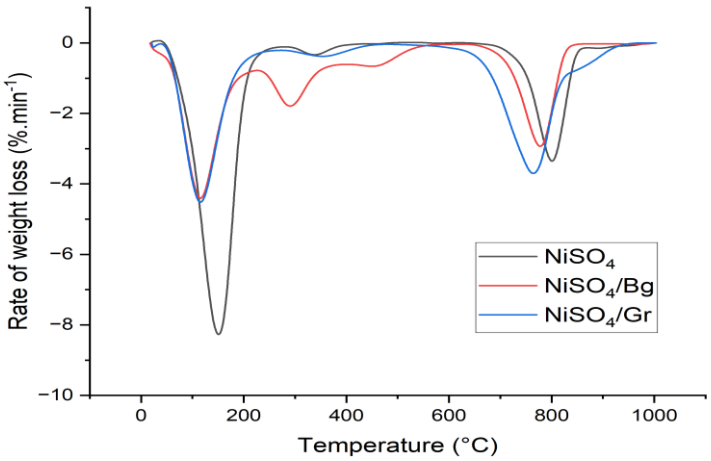

Figure 15. DTG measurements of the decomposition of $NiSO_4.6H_2O$ with graphite and sugarcane Bagasse.

The most significant change occurs between 600°C and 800°C, where the presence of graphite promotes the reduction of $NiSO_4$ to NiO. This is evident from the sharp mass loss observed in the TG curve and the distinct peak in the DTG curve, which reflect an accelerated decomposition process. However, the reported downward shift in the onset temperature of $NiSO_4$ decomposition by approximately 120–200°C appears to be overestimated. A more precise comparison is needed. We recommend analyzing the initial and final desulfation temperatures more rigorously—ideally, by tabulating

these values across different samples to clearly illustrate the shifts. Both graphite and sugarcane bagasse influence the kinetics of desulfation, although the effect of graphite is notably more pronounced. Comparing these results with the TGA profiles of the pure additives (graphite and sugarcane bagasse) would provide further insight into the observed phenomena. In the case of graphite, gasification and CO formation begin around 600°C, overlapping with the main decomposition range of $NiSO_4$. For sugarcane bagasse, gasification is expected to have completed by this point; however, it is possible that residual biomass forms char, which could subsequently undergo gasification in a similar temperature range as graphite. This reduction in temperature suggests a chemical interaction beyond simple heat dispersion effects. According to Miao et al. (53) and Tao et al. (54)expanded graphite (EG) influences thermal decomposition primarily through its high thermal conductivity, which improves heat transfer and accelerates decomposition. However, in the present study, the effect is not solely physical but also chemical. Graphite acts as a reductant, either through direct solid-state reduction or via the formation of CO, which lowers the local O_2 partial pressure and significantly alters the kinetics of sulfate decomposition—making this system notably different from previously studied cases. This effect can be further clarified with chemical equations. One possible pathway involves the reduction of $NiSO_4$ by CO:

$$NiSO_4 + CO \rightarrow NiO + CO_2 + SO_3 \quad (29)$$

Alternatively, graphite may first react with residual oxygen to form CO, which then indirectly facilitates the decomposition. Both mechanisms are plausible and should be discussed to fully understand the role of graphite in modifying the decomposition environment and reaction pathway.

Table 7. The theoretical, experimental values of mass loss of Pure Nickel sulfate with graphite

Reaction	Temperature (°C)	Mass Loss (%) – Found	Mass Loss (%) – Calculated
Equation 25	135.6	14.2	13.10
Equation 26	167.7	20.12	19.66
Equation 27	315.5	7.5	6.55
Equation 28	815.3	32.40	33.50

The thermal decomposition of 70% $NiSO_4 \cdot 6H_2O$ with 30% sugarcane bagasse, shown in Figure 14, follows distinct weight loss stages associated both dehydration and biomass decomposition. Unlike pure sugarcane bagasse, which begins degrading around 200°C, the $NiSO_4$–bagasse mixture starts losing mass at ~160°C, indicating an interaction between the two components. Pure bagasse in figure 11 undergoes three main stages: moisture evaporation (up to 150°C, 8–12% loss), biomass decomposition (200–450°C, 50–60% loss), and char formation (above 450°C, final weight ~20%).(59,60) In contrast, the $NiSO_4$–bagasse mixture exhibits a higher initial weight loss (~10–15%) due to $NiSO_4 \cdot 6H_2O$ dehydration and a more controlled biomass decomposition (45–55% loss), suggesting $NiSO_4$ influences the release of volatiles. Above 450°C, pure bagasse retains ~20% of its weight, whereas the $NiSO_4$–bagasse system shows an 80–85% reduction, indicating enhanced decomposition.

The bagasse acts as a reducing agent, likely forming CO, which lowers the local O_2 partial pressure and accelerates $NiSO_4$ decomposition. The shift in DTG peak temperatures further confirms this effect. The main thermal events occurred at temperatures between 120 to 600 °C and corresponded to the breaking of the side chain of lignin molecules which released H_2O, CO, and CO_2 gases. The thermal event that occurred at a temperature > 600 °C was primarily attributed to the evolution of CO, CO_2, and CH_4.(61,62)

4.4. Kinetic Modelling

4.4.1. Magnesium Sulfate thermal decomposition

Figures 16 and 17 present the linear regression analysis and experimental (TGA) data, along with the sigmoidal fitting for the desulfation thermal event observed for pure magnesium sulfate. The sigmoidal model fits the experimental data quite well, as indicated by the coefficient of determination (R^2) value of 0.995 and attested for the significant proximity of the model and experimental curves.

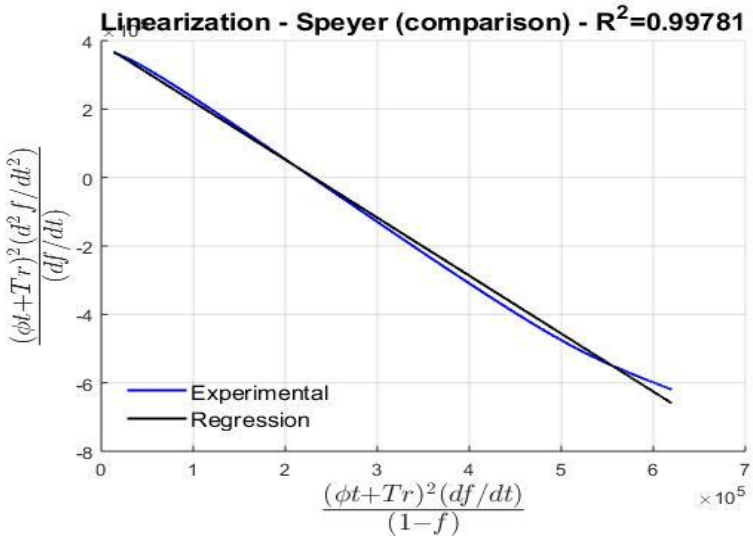

Figure 16. Linear regression analysis applied for magnesium sulfate.

These facts suggest that the mathematical model correctly describes the behavior of the thermogravimetric curve. However, although the R^2 values indicate an excellent fit of the model to the experimental points, a graphical visualization of the fitting is essential to confirm this fit, and it can be clearly observed that the sigmoidal function proposed is considerably near than the experimental curve between 1300 and 1350 K, but deviates appreciably from experimental data either at the beginning or end of the thermal event evidenced.

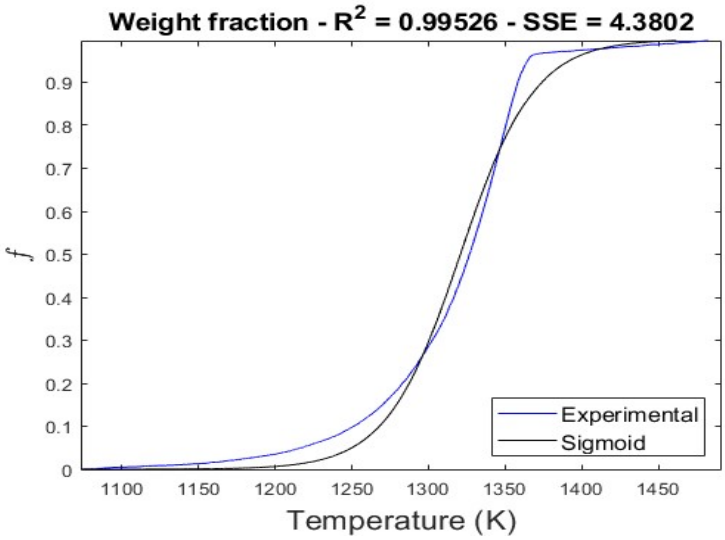

Figure 17. Experimental and sigmoidal approximation values of weight fraction $MgSO_4.7H_2O$.

It could be speculated that the difficulty in fitting evolves from the fact that, according to thermodynamic simulations, the monohydrate sulfate ($MgSO_4.H_2O$) is steel present and contributes for the overall mass loss measured. This fact leads to deviations from sigmoidal shape. Through use of Equation 9, the activation energy (Ea) for the decomposition of magnesium sulfate heptahydrate was determined to be 321.93 $kJ.mol^{-1}$, which is relatively high. This suggests that the decomposition of $MgSO_4.7H_2O$ is a thermally demanding process, requiring a significant amount of energy to overcome the activation barrier, which is consistent with the fact that the anhydrous sulfate is a phase of considerable thermodynamic stability, as demonstrated by the simulations presented before (Figure 6). The obtained Ea value aligns well with previous studies, by Hulber (21) (343.1 $kJ.mol^{-1}$), L'vov and Ugolkov (22) (311.7 $kJ.mol^{-1}$), and Brownell (36) (335.7 $kJ.mol^{-1}$). Additionally, the observed non-integer result of 1.6940 for the reaction order indicates that the this suggests that the decomposition of $MgSO_4$ does not strictly follow a simple first- or second-order mechanism. Instead, it likely involves a more complex reaction pathway, possibly governed by a combination of surface reactions and diffusion processes. This intermediate kinetic order may also indicate overlapping mechanisms, such as a transition from chemically controlled to diffusion-controlled stages during thermal

decomposition. Such a result is consistent with the findings of Souza et al.(45), showed similar results, studied the thermodynamics simulations and kinetics modeling of the thermal decomposition of $MgSO_4.7H_2O$ with reducing agent effect like graphite, charcoal and coke, and he found activation energy from 22 to 340 $kJ.mol^{-1}$ with reaction order 1.8 to 1.6.

Figures 18 and 19 illustrate the weight fraction of $MgSO_4 \cdot 7H_2O$ with graphite, incorporating both experimental linear regression and sigmoidal approximation. The determination coefficient, activation energy, and apparent reaction order for each sample are provided in Table 8.

The reaction order n decreases slightly, from 1.6940 for pure $MgSO_4 \cdot 7H_2O$ to values around 1.35-1.39 for the mixtures with graphite. This suggests that the graphite reduces the influence of $MgSO_4 \cdot 7H_2O$ concentration on the reaction rate, potentially indicating a change in the reaction mechanism due to graphite's presence. The activation energy decreases significantly from 321.93 $kJ \cdot mol^{-1}$ for pure $MgSO_4 \cdot 7H_2O$ to approximately 80–101 $kJ \cdot mol^{-1}$ with the addition of graphite. This substantial reduction in Ea suggests that graphite facilitates the decomposition process by lowering the energy barrier required for the reaction to proceed, potentially acting as a catalyst or providing an alternative reaction pathway. A similar observation was reported by Hlabela et al.(63), who determined an activation energy of 149 ± 10 $kJ \cdot mol^{-1}$ for the reduction of barium sulfate to barium sulfite in the presence of carbon monoxide using isothermal thermogravimetric analysis, highlighting how the presence of a reducing agent can influence the reaction kinetics. Plewa and Steindor (16) reported an activation energy of 209.7 $kJ \cdot mol^{-1}$ for the isothermal decomposition of $MgSO_4$ in the presence of CO (640–665 °C, oxidizing atmosphere) using a shrinking-core model. In contrast, our experiments with graphite yielded much lower Ea values (80–101 $kJ \cdot mol^{-1}$), indicating that graphite is even more effective than CO at reducing the energy barrier for $MgSO_4 \cdot 7H_2O$ decomposition—likely by providing a superior catalytic surface or an alternative, lower-energy reaction pathway. Lastly, the R^2 values are high, ranging from 0.998 to 0.986, indicating that the kinetic model fits the experimental data well, with only a slight decrease in fit quality as more graphite is added.

Table 8 Kinetic parameters and R2 values of the decomposition of magnesium sulfate and graphite mixtures

Samples	n	E_a (kJ.mol^{-1})	R^2
$MgSO_4.7H_2O$	1.6940	321.93	0.998
90%$MgSO_4.7H_2O$ +10%Graphite	1.3906	80.68	0.9941
80%$MgSO_4.7H_2O$ +20%Graphite	1.3647	100.23	0.9884
70%$MgSO_4.7H_2O$ +30%Graphite	1.3482	101.82	0.986

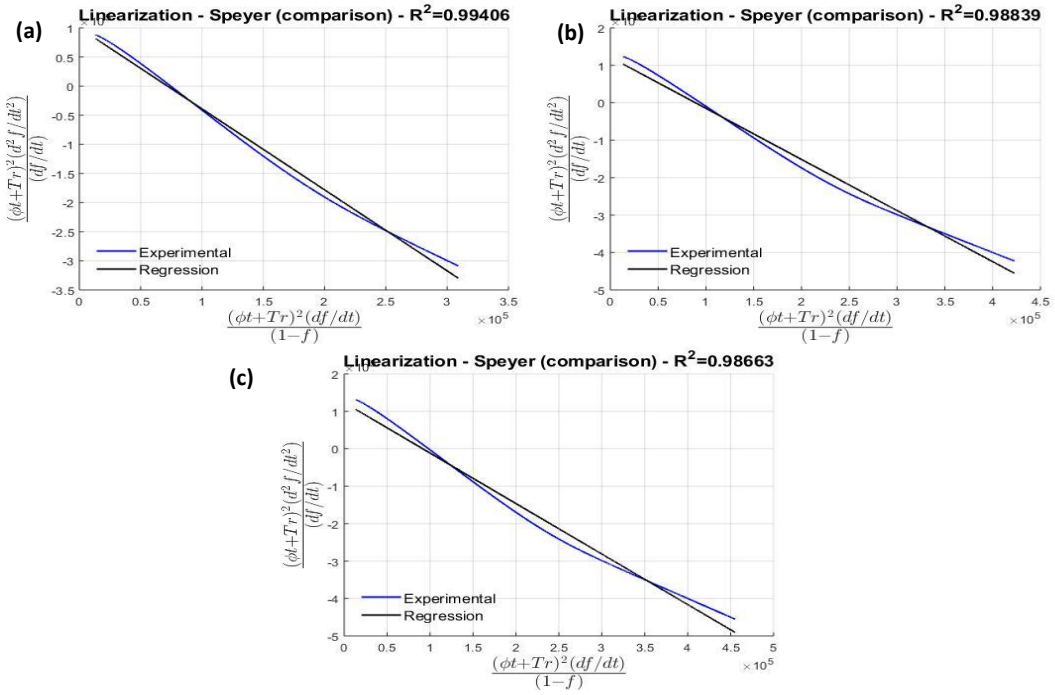

Figure 18. Linear regression analysis applied for (a) 90% $MgSO_4.7H_2O$ +10%Graphite (b) 80% $MgSO_4.7H_2O$ +20%Graphite (c) 70% $MgSO_4.7H_2O$ +30%Graphite.

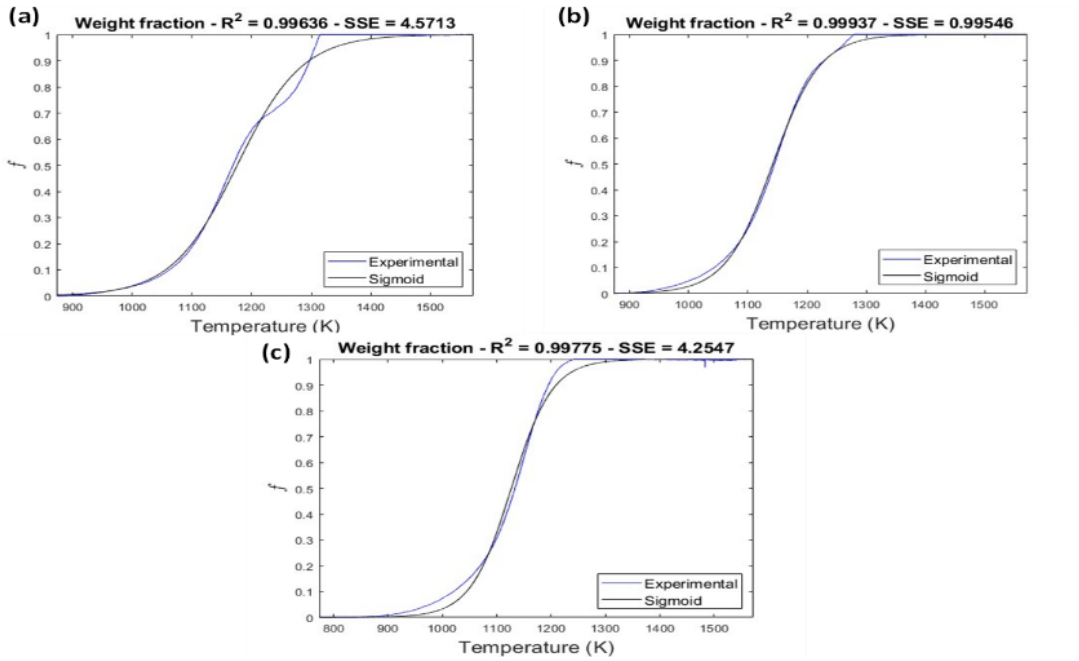

Figure 19. Experimental and sigmoidal approximation values of weight fraction (a) 90% $MgSO_4.7H_2O$ +10%Graphite (b) 80% $MgSO_4.7H_2O$ +20%Graphite (c) 70% $MgSO_4.7H_2O$ +30%Graphite.

To ensure the validity of these observations, it is necessary to confirm whether the nature of the samples is correctly identified. Interestingly, the samples with higher graphite content exhibit a curve shape more like that of the pure sample, raising the possibility of a misidentification issue. One possible explanation for this behavior is the formation of CO_2 through a sequence of reactions involving CO generated from graphite. During sulfate decomposition, SO_3 may decompose to SO_2 and release oxygen. The released O_2 can then react with CO (from graphite gasification) to form CO_2. This series of reactions alters the local gas environment and may influence the decomposition pathway. Another potential explanation is the direct reaction between $MgSO_4$ and the carbon present in graphite.

The activation energy for pure $MgSO_4 \cdot 7H_2O$ was reported as 322.731 $kJ \cdot mol^{-1}$, following a first-order reaction. The addition of carbon-based reducing agents significantly increased the activation energy, with values of 340.391 $kJ \cdot mol^{-1}$ for green coke, 196.120 $kJ \cdot mol^{-1}$ for graphite, 191.100 $kJ \cdot mol^{-1}$ for coke breeze, and 162.302 $kJ \cdot mol^{-1}$ for charcoal.(45) The global reaction order of 1.36 suggests a complex

decomposition mechanism, potentially involving interactions between carbon and oxygen released during sulfate decomposition. However, this explanation must be refined, as it appears to contradict the higher activation energy values reported earlier. In the case of $MgSO_4$, the decomposition likely generates CO as the reducing species rather than CO_2. Rather than lowering the activation energy, the interaction between CO and residual graphite may contribute to a more intricate reaction pathway, possibly increasing energy demands due to competing or overlapping processes.

At high temperatures, CO_2 molecules require significant kinetic energy and interact weakly with carbon, as chemisorption becomes negligible. This allows the reaction to be governed by gasification kinetics, in which CO becomes the dominant reactive species. This explains why the addition of graphite leads to a lower activation energy, as it enhances the thermal decomposition process. These findings are supported by previous studies (64,65,66), which suggest that the presence of graphite or other carbon-based materials can facilitate formation of oxides through reaction of in-situ generated reducing agents with sulfate crystals, thereby lowering activation energies and accelerating the reaction involved. The reduction in activation energy observed in this study has broader implications for systems that require lower activation energies for efficient processing or reaction. The use of graphite as a reducing agent could be beneficial in industrial applications where energy savings and enhanced reaction rates are desired, particularly for processes involving the thermal decomposition of magnesium sulfate or similar compounds. In contrast, the use of sugarcane bagasse did not produce comparable effects under the tested conditions, suggesting that its role as a reductant is limited or less effective in this context. This highlights the importance of selecting suitable carbon sources based on their thermal reactivity and interaction with decomposition products.

4.4.2. Nickel Sulfate thermal decomposition

Figures 20 and 21 illustrate the complex decomposition mechanism of nickel sulfate hexahydrate, as evidenced by its non-integer reaction order of 1.2734. This suggests that the process does not follow a simple first-order reaction but instead

involves multiple stages or overlapping reactions. According to the present results, the global activation energy for the decomposition of $NiSO_4 \cdot 6H_2O$ was determined to be 130.045 $kJ \cdot mol^{-1}$, which is significantly lower than that of magnesium sulfate heptahydrate (321.93 $kJ \cdot mol^{-1}$). This lower energy requirement indicates that $NiSO_4 \cdot 6H_2O$ is thermally less stable and decomposes more readily than $MgSO_4 \cdot 7H_2O$. Thermodynamically, this behavior can be attributed to weaker bond strengths and less stable hydration shells in $NiSO_4 \cdot 6H_2O$, leading to a lower decomposition temperature. Tomaszewicz et al.(19) reported a multi-stage decomposition of $NiSO_4 \cdot 6H_2O$ under oxidative atmosphere, with activation energies of 58.5, 117.0, and 179.0 $kJ \cdot mol^{-1}$ for the respective stages, using the Coats-Redfern method. The global activation energy obtained in this study (130.045 $kJ \cdot mol^{-1}$) falls within this range, supporting the multi-step nature of the decomposition and validating the consistency of the present findings with the literature. As indicated by the earlier discussion, the thermodynamic driving forces for the decomposition of $NiSO_4 \cdot 6H_2O$ are more favorable, which contributes to its lower activation energy and easier breakdown compared to $MgSO_4 \cdot 7H_2O$.

The coefficient of determination $R^2 = 0.9768$ suggests that the sigmoidal model fits the experimental data well, though not as perfectly as in the case of $MgSO_4 \cdot 7H_2O$, which had an R^2 value of 0.995. The significant deviation in the fit may result from the presence of intermediate phases or additional thermal effects during decomposition, which can complicate the overall reaction pathway. Literature suggests that intermediate oxisulfates, such as those observed in the thermal decomposition of $ZnSO_4$ as discussed in previous article(67), could play a similar role here. These phases might contribute to the observed deviations in the thermal data. Alternatively, issues during analysis, such as incomplete sample preparation or equipment limitations, could also explain the discrepancies. To better understand the underlying processes, it would be valuable to characterize the material produced at specific temperatures during the decomposition. This could provide insights into the formation of intermediate phases and help clarify the observed deviations in the thermal behavior.

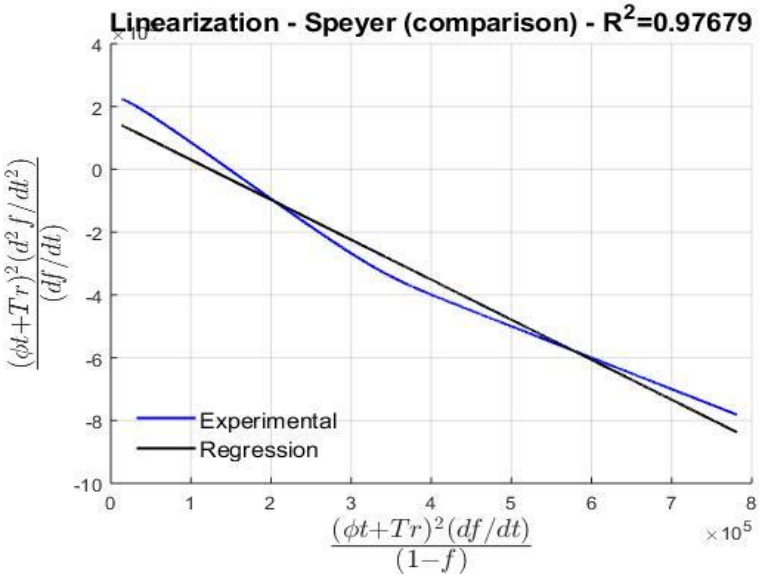

Figure 20. Linear regression analysis applied for Nickel sulfate

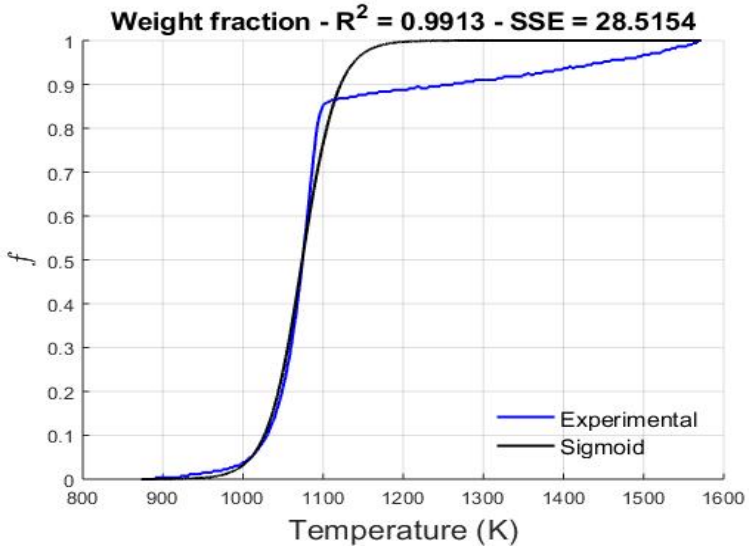

Figure 21. Experimental and sigmoidal approximation values of weight fraction $NiSO_4.6H_2O$

The linear regression and Experimental and sigmoidal of 70% $NiSO_4 \cdot 6H_2O$ with 30% graphite in figure 22 and 23 exhibits notable changes compared to pure $NiSO_4 \cdot 6H_2O$, particularly in terms of E_a, n, and R^2 values are displayed in Table 9. The presence of graphite significantly lowers the activation energy for the decomposition of $NiSO_4 \cdot 6H_2O$ from 130.045 $kJ \cdot mol^{-1}$ to 82.62 $kJ \cdot mol^{-1}$. This notable reduction in the energy barrier suggests that graphite plays a substantial role in facilitating the reaction,

likely enhancing the formation of NiO by acting as a reducing agent or providing an alternative reaction pathway. A comparable effect was observed by Hlabela et al.(68), who reported an activation energy of $149 \pm 10\ \mathrm{kJ \cdot mol^{-1}}$ for the reduction of barium sulfate to barium sulfite in the presence of carbon monoxide, using isothermal thermogravimetric analysis. Their study similarly highlighted the influence of a reducing atmosphere in lowering the energy requirements of sulfate decomposition reactions.

Table 9. Kinetic parameters and R^2 values of the decomposition of Nickel sulfate and graphite mixtures.

Samples	n	E_a (kJ.mol^{-1})	R^2
$NiSO_4.6H_2O$	1.2734	130.045	0.9768
70%$NiSO_4.6H_2O$ +30%Graphite	1.22	82.62	0.9814

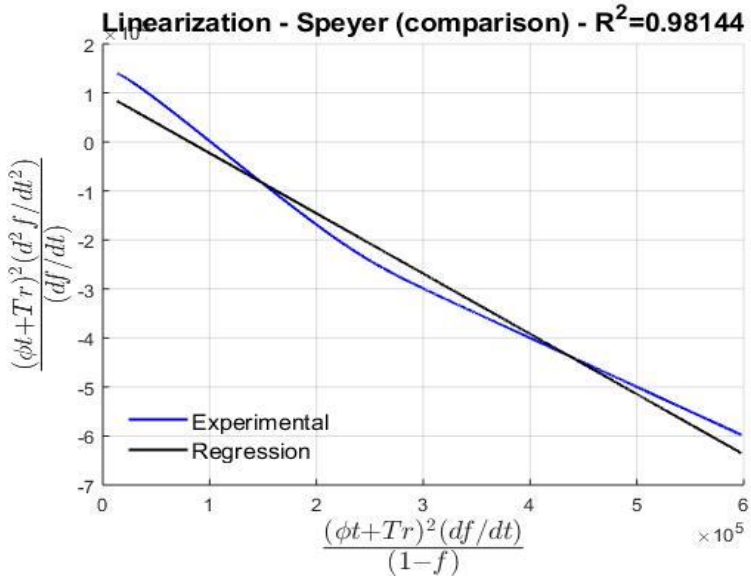

Figure 22. Linear regression analysis applied for 70% $NiSO_4.6H_2O$ +30%Graphite.

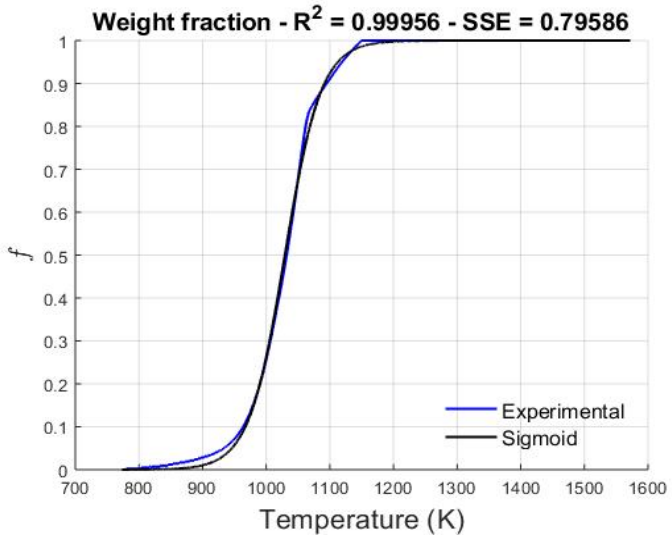

Figure 23. Experimental and sigmoidal approximation values of weight fraction 70% $NiSO_4.6H_2O$ +30%Graphite.

One of the primary reasons for this effect is graphite's high thermal conductivity, which enables efficient heat transfer throughout the sample. In pure $NiSO_4 \cdot 6H_2O$, decomposition occurs in a system where heat is transferred relatively slowly, resulting in uneven heating and potential thermal resistance effects.(37) Therefore, in the graphite-containing mixture, heat is distributed more uniformly due to the conductive nature of graphite. This prevents localized overheating, allowing for a more controlled and consistent reaction pathway, thereby reducing variations in the kinetic parameters. Additionally, graphite plays a key role in the chemical aspects of the decomposition process. As the temperature increases, graphite plays a crucial role in facilitating the partial reduction of $NiSO_4$ to NiO, primarily through CO formation. This effect is much more significant than the contribution of graphite's thermal conductivity, which has a lesser impact on the overall reaction. The reduction mechanism is driven by CO, which is generated from graphite as it undergoes gasification at elevated temperatures. The CO then interacts with $NiSO_4$, reducing it to NiO and releasing SO_2 and CO_2. This process not only accelerates the decomposition of $NiSO_4$ but also alters the local gas environment, enhancing the overall efficiency of the reaction. The influence of graphite on the reduction mechanism significantly surpasses any potential role it might have in improving heat transfer, making it a dominant factor in the thermal decomposition of $NiSO_4$.The reaction order (n = 1.22),

which is higher than unity, suggests, as in the case of magnesium sulfate containing samples, that a non-elementary reaction is involved. Previous studies (69,64,65) support these findings, indicating that graphite and other carbon-based materials can enhance compound decomposition by reducing activation energies and speeding up the reaction.

Figures 24 and 25 illustrate the linear regression and sigmoidal fitting of $NiSO_4 \cdot 6H_2O$ in the presence of sugarcane bagasse. The thermal decomposition of a 70% $NiSO_4 \cdot 6H_2O$ and 30% sugarcane bagasse (SCB) mixture resulted in a slight reduction in activation energy (E_a = 123.74 kJ·mol^{-1}) compared to pure $NiSO_4 \cdot 6H_2O$ (130.045 kJ·mol^{-1}). This suggests that SCB has a mild influence on the decomposition process, possibly due to its partial reducing ability or interaction with the sulfate matrix, though its effect is notably weaker than that of graphite. This finding is consistent with previous studies on sugarcane biomass, where multi-stage decomposition behavior was reported. In particular, a TG-based kinetic study of sugarcane bagasse reported activation energies ranging from 56 to 350 kJ·mol^{-1} for different decomposition steps in both inert and oxidative atmospheres, with values of 130 kJ·mol^{-1} overlapping with those observed in the present study.(70).Sugarcane bagasse influences the decomposition process but to a lesser extent than graphite. There are two possible reasons for this: first, the temperature range at which in-situ reducing agent molecules are formed might be different for bagasse compared to graphite, with bagasse likely forming reducing agents at higher temperatures (as we clearly see in the TGA figure 11 of pure sugarcane bagasse). Second, the amount of reducing agents produced from bagasse may be lower than that generated by graphite, reducing its effectiveness in promoting the decomposition process.

The reaction order (n = 1.223) remains close to that of pure $NiSO_4 \cdot 6H_2O$ (Table 10), suggesting that while bagasse alters the decomposition mechanism, it does not significantly accelerate the reaction rate.

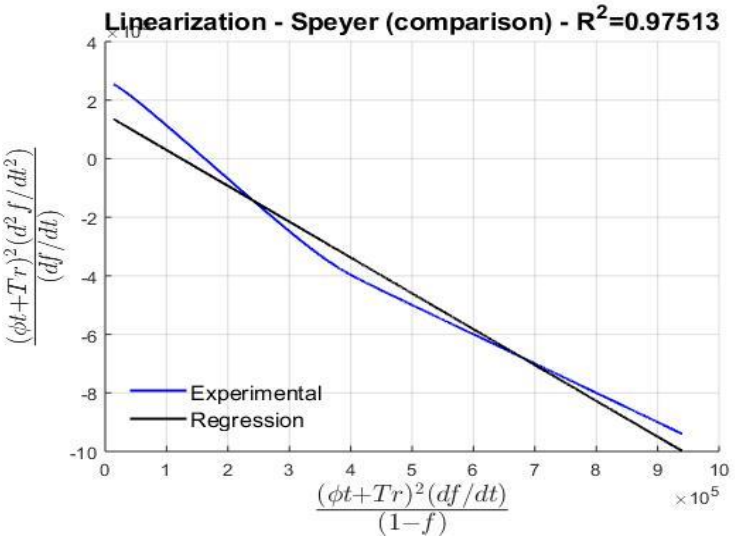

Figure 24. Linear regression analysis applied for 70% $NiSO_4.6H_2O$ +30%Sugarcane Bagasse

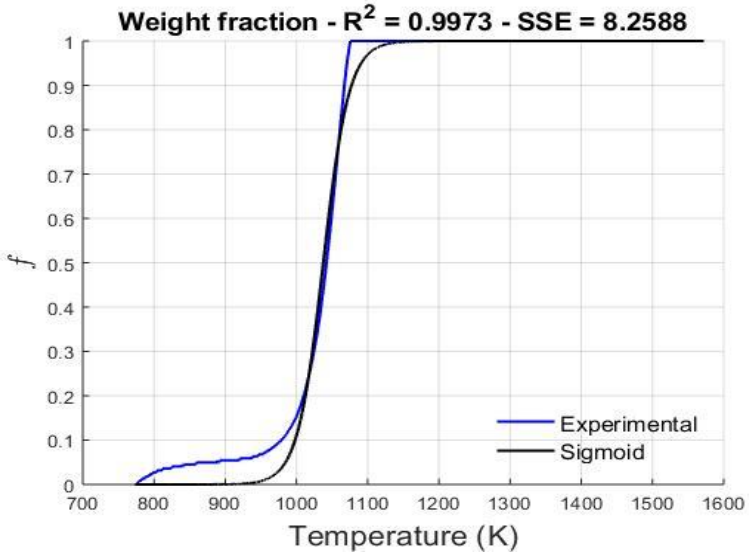

Figure 25. Experimental and sigmoidal approximation values of weight fraction 70% $NiSO_4.6H_2O$ +30%Sugarcane Bagasse.

Table 10. Kinetic parameters and R^2 values of the decomposition of Nickel sulfate and sugarcane mixture

Samples	n	E_a (kJ.mol^{-1})	R^2
$NiSO_4.6H_2O$	1.2734	130.045	0.9768
70%$NiSO_4.6H_2O$ +30%Sugarcane Bagasse	1.223	123.74	0.975

Unlike graphite, which consistently facilitates the reduction process through the formation of CO, biomolecules contained in bagasse react with the available O_2 in the atmosphere, leading to a much more complex and variable reaction environment. The reactions involving bagasse are less straightforward and more influenced by the composition of the biomass, resulting in a less predictable impact on the decomposition process compared to graphite's more direct role. Despite these variations, the overall kinetic model still provides a good fit, confirming that the presence of bagasse modifies but does not drastically change the thermal decomposition behavior. This result closely relates to the pyrolytic study of metal-impregnated sugarcane bagasse using isoconversional models (FWO, KAS, Kissinger's), where Ni, Ru, and Fe reduced activation energy (SB-Ni: 62.50 $kJ.mol^{-1}$, SB-Ru: 78.46 $kJ.mol^{-1}$, SB-Fe: 83.09 $kJ.mol^{-1}$) and influenced thermal degradation. (30)

5 Conclusion

This study investigated the thermal decomposition kinetics of magnesium sulfate heptahydrate ($MgSO_4 \cdot 7H_2O$) and nickel sulfate hexahydrate ($NiSO_4 \cdot 6H_2O$) in the presence of graphite and sugarcane bagasse as carbon source. Through non-isothermal thermogravimetric analysis, the study provided a detailed understanding of the stepwise dehydration process and the subsequent decomposition of anhydrous sulfates into metal oxides and gaseous sulfur species. The results highlighted the significant influence of graphite in lowering the decomposition temperature and accelerating reaction kinetics, whereas sugarcane bagasse exhibited a weaker impact on the process.

Thermodynamic equilibrium simulations revealed distinct decomposition pathways for magnesium sulfate and nickel sulfate. For magnesium sulfate, the simulations indicated a progressive dehydration sequence, ultimately leading to the formation of anhydrous $MgSO_4$ and further MgO. The presence of graphite significantly altered the equilibrium conditions by shifting the decomposition temperature to a lower range (~340°C), enhancing the sulfate reduction process.

In contrast, nickel sulfate exhibited a higher thermal stability, with dehydration occurring in sequential steps until anhydrous $NiSO_4$ and decomposed into NiO. When graphite was introduced, $NiSO_4$ decomposition was facilitated at lower temperatures (~600°C), and the suppression of SO_3 formation was observed, indicating a shift in the gas-phase equilibrium.

The thermal analysis of pure magnesium sulfate and its mixtures with graphite and sugarcane bagasse provides valuable insights into their decomposition behavior. Adding graphite influences the decomposition process by lowering the onset decomposition temperature. The DTG curves reveal that in the presence of graphite, the decomposition of anhydrous $MgSO_4$ occurs at a lower temperature (900°C) compared to pure $MgSO_4$ (1050°C), demonstrating the catalytic role of carbon. On the other hand, the incorporation of sugarcane bagasse did not significantly alter the dehydration pathway of $MgSO_4 \cdot 7H_2O$, as evidenced by similar mass loss patterns in the TGA curve.

The TGA and DTG analyses of pure nickel sulfate and its mixtures with graphite and sugarcane bagasse reveal distinct thermal decomposition behaviors. The addition of graphite significantly alters the decomposition pathway of nickel sulfate. The presence of graphite lowers the onset temperature of $NiSO_4$ decomposition by approximately 120–200°C. The DTG curves highlight a sharp mass loss between 600°C and 800°C, suggesting that graphite facilitates the reduction of $NiSO_4$ to NiO. Similarly, the thermal decomposition of $NiSO_4 \cdot 6H_2O$ mixed with sugarcane bagasse follows a distinct pattern. The TGA curve shows that the presence of $NiSO_4$ shifts the onset of bagasse decomposition to ~300°C, indicating an interaction between the sulfate and the organic components.

The kinetic modeling provided further insight into the reaction mechanisms governing sulfate decomposition by evaluating the activation energy and reaction order, which are key parameters in determining the rate-controlling step of the process. For magnesium sulfate, the activation energy (Ea) values demonstrated a significant reduction when graphite was introduced as a reducing agent. The activation energy for pure $MgSO_4$ was found to be 321.93 $kJ.mol^{-1}$, indicating a high energy barrier for decomposition in the absence of a reducing agent. However, when 10% graphite was added to the system, the activation energy dropped drastically to 82.62 $kJ.mol^{-1}$. Further increases in the graphite content resulted in activation energies of 100.23 $kJ.mol^{-1}$for an 80%-20% mixture and 101.82 $kJ.mol^{-1}$for a 70%-30% mixture, suggesting a saturation effect beyond a certain graphite concentration. The reaction order was determined to be approximately 1.36, which is characteristic of a chemically controlled reaction mechanism.

Nickel sulfate exhibited a distinct kinetic behavior compared to magnesium sulfate, with activation energy values varying significantly depending on the reducing agent used. In the absence of a reducing agent, the decomposition of $NiSO_4$ exhibited an activation energy of 130.04 $kJ.mol^{-1}$. When graphite was introduced as a reducing agent, the activation energy significantly decreased to 82.62 $kJ.mol^{-1}$ for a 70%-30% $NiSO_4 \cdot 6H_2O$-graphite mixture. When sugarcane bagasse was used as a reducing agent, the activation energy decreased to 123.74 $kJ.mol^{-1}$for a 70%-30% $NiSO_4 \cdot 6H_2O$-sugarcane bagasse mixture. This decrease suggests that sugarcane

bagasse provides some reduction capability, but it is not as effective as graphite in lowering the energy barrier for sulfate decomposition. Unlike $MgSO_4$, which exhibits a strong response to the presence of a reducing agent in lowering activation energy, $NiSO_4$ decomposition is influenced to a lesser extent. This suggests that nickel sulfate reduction may involve additional kinetic barriers or require more reactive reducing agents to achieve a significant catalytic effect.

The study's findings highlight the crucial role of in-situ generated reducing in modifying the thermal decomposition behavior of metal sulfates. Graphite was shown to significantly alter equilibrium conditions, reduce decomposition temperatures, and enhance sulfate reduction efficiency. These insights are particularly relevant for industrial applications where energy efficiency and process optimization are critical. The suppression of SO_3 formation in nickel sulfate decomposition has additional environmental implications, as it could lead to reduced sulfur emissions and cleaner process outputs.

5.1. Future work

Several avenues for future research are proposed to build upon the findings of this study and address existing gaps in the understanding of magnesium and nickel sulfate decomposition kinetics:

1. **Influence of Heating Rates and Hydration States:** Future studies should explore the effect of different heating rates on the decomposition kinetics of $MgSO_4$ and $NiSO_4$. Additionally, experiments should be conducted with different hydration states of magnesium sulfate (e.g., monohydrate, hexahydrate) to understand their influence on thermal stability and reaction pathways.
2. **Reactivity of Alternative Reducing Agents**: Further investigations could focus on the interaction of decomposition products with alternative reducing agents beyond carbonaceous materials. Exploring metals, metal oxides, or other novel reductants could provide insights into optimizing sulfate reduction efficiency under different conditions.

3. **Decomposition Behavior of Industrial Residues**: Future research should focus on the thermal decomposition of magnesium sulfate within industrial residues rather than pure sulfate. These residues, often containing impurities such as iron, manganese, and calcium, may influence thermal stability and kinetic parameters, impacting process efficiency. Investigating real-world waste streams could provide more applicable insights for industrial applications

4. **Advanced Kinetic Modeling Using Optimization Algorithms:** To improve the accuracy of kinetic parameter estimation, a more advanced modeling approach based on the Particle Swarm Optimization (PSO) algorithm should be implemented. This technique would allow for more precise determination of activation energy (Ea) and reaction order (n), providing a deeper understanding of the chemical control mechanisms governing decomposition.

5. **Characterization of Solid Mixtures During Decomposition:** The mixtures containing sugarcane bagasse and magnesium sulfate should be analyzed during different stages of thermal decomposition using XRD and SEM/EDS techniques to identify the presence of residual carbon and potential reaction intermediates.

6. **Isothermal Kinetic Studies:** Complementary kinetic studies under isothermal conditions should be performed to compare dynamic (non-isothermal) and steady-state (isothermal) conditions. The results could provide further insights into the heat transfer effects on kinetic parameters.

7. **Exploration of Alternative Kinetic Models:** To further validate the kinetic findings, future research should apply alternative modeling approaches beyond the Vaschuska method. Models such as the Avrami-Erofeev equation, the Prout-Tompkins model, or the Coats-Redfern method could offer new insights into reaction mechanisms and the influence of heat and mass transfer on decomposition kinetic.

6 Bibliography

[1] AL-TABBAA, A. Reactive magnesia cement. Em: **Eco-efficient concrete**. [s.l.] Elsevier, 2013. p. 523–543.

[2] YAROSHEVSKY, A. A. Abundances of chemical elements in the Earth's crust. **Geochemistry International**, v. 44, p. 48–55, 2006.

[3] HABASHI, F. **Handbook of extractive metallurgy**. Wiley-VCH, , 1997.

[4] PINTO, R. D. E. S. ENERGIA NUCLEAR NA MATRIZ ENERGETICA BRASILEIRA. [s.d.].

[5] DA SILVA, A. M. V. Estudos sobre a recuperação do titânio contido no rejeito da concentração de magnetita. 2018.

[6] SCHEIDEMA, M. The reaction mechanism and operating window for the decomposition of hydrated magnesium sulfate under reducing conditions. 2015.

[7] BONELLO, G.; BERTHET, P.; D'HENDECOURT, L. **Identification of magnesium sulfate hydration state derived from NIR reflectance spectroscopy**. 36th Annual Lunar and Planetary Science Conference. **Anais**...2005.

[8] PHADNIS, A. B. ON THE DEHYDRATION OF MGSO47H2O. 1981.

[9] EMONS, H.-H. et al. Thermal decomposition of the magnesium sulphate hydrates under quasi-isothermal and quasi-isobaric conditions. **Journal of Thermal Analysis and Calorimetry**, v. 36, n. 4, p. 1265–1279, 1990.

[10] SEEGER, M. et al. Magnesium compounds. **Ullmann's Encyclopedia of Industrial Chemistry**, 2000.

[11] NICHOLLS, D. **The chemistry of iron, cobalt and nickel: comprehensive inorganic chemistry**. [s.l.] Elsevier, 2013. v. 24

[12] STEELE, B. D.; JOHNSON, F. M. G. XIII.—The solubility curves of the hydrates of nickel sulphate. **Journal of the Chemical Society, Transactions**, v. 85, p. 113–120, 1904.

[13] INGRAHAM, T. R. THERMODYNAMICS OF THE THERMAL DECOMPOSITION OF NICKEL--2-- SULFATE.. THE NI-S-O SYSTEM

FROM 1000 TO 1150 K. **AIME MET SOC TRANS**, v. 236, n. 7, p. 1064–1067, 1966.

[14] EDWARDS, B. P. Energy use in cane and beet factories. 1991.

[15] ISLAM, M. R.; PARVEEN, M.; HANIU, H. Properties of sugarcane waste-derived bio-oils obtained by fixed-bed fire-tube heating pyrolysis. **Bioresource Technology**, v. 101, n. 11, p. 4162–4168, 2010.

[16] PLEWA, J.; STEINDOR, J. Kinetics of reduction of magnesium sulfate by carbon oxide. **Journal of thermal analysis**, v. 32, p. 1809–1820, 1987.

[17] SCHEIDEMA, M. N.; TASKINEN, P. Decomposition thermodynamics of magnesium sulfate. **Industrial & engineering chemistry research**, v. 50, n. 16, p. 9550–9556, 2011.

[18] DA GUARDA SOUZA, M. O.; REBOUCAS, L. M.; DE CASTRO, L. M. F. Characterization and thermal decomposition study of mango residue biomass (Mangifera indica L.). **Journal of Thermal Analysis and Calorimetry**, v. 139, n. 3, p. 1811–1816, 2020.

[19] TOMASZEWICZ, E.; KOTFICA, M. Mechanism and kinetics of thermal decomposition of nickel (II) sulfate (VI) hexahydrate. **Journal of thermal analysis and calorimetry**, v. 77, p. 25–31, 2004.

[20] STRASZKO, J.; MOŻEJKO, J.; OLSZAK-HUMIENIK, M. Kinetics of thermal decomposition of nickel sulfate hexahydrate. **Journal of Thermal Analysis and Calorimetry**, v. 45, n. 5, p. 1109–1116, 1995.

[21] HULBERT, S. F. Effect of processing parameters on the kinetics of decomposition of magnesium sulphate. **Materials Science and Engineering**, v. 2, n. 5, p. 262–268, 1968.

[22] L'VOV, B. V; UGOLKOV, V. L. Kinetics of free-surface decomposition of magnesium and barium sulfates analyzed thermogravimetrically by the third-law method. **Thermochimica acta**, v. 411, n. 1, p. 73–79, 2004.

[23] DE MELLO, K. et al. Multiscale land use impacts on water quality: Assessment, planning, and future perspectives in Brazil. **Journal of Environmental Management**, v. 270, p. 110879, 2020.

[24] ROCHE, E. G.; PRASAD, J. Magnesium oxide recovery. **WO Patent**, v. 2007070973, 2007.

[25] SOUZA, B. et al. MgSO4 carbothermic reductive decomposition to produce a highly reactive MgO powder. **Journal of Materials Research and Technology**, v. 9, n. 2, p. 1847–1855, 2020.

[26] BROWN, R. C. **Thermochemical processing of biomass: conversion into fuels, chemicals and power**. [s.l.] John Wiley & Sons, 2019.

[27] LV, X. et al. Non-isothermal kinetics study on carbothermic reduction of nickel laterite ore. **Powder Technology**, v. 340, p. 495–501, 2018.

[28] XIA, X. et al. Recovery of CaO from CaSO4 via CO reduction decomposition under different atmospheres. **Journal of Environmental Management**, v. 301, p. 113855, 2022.

[29] ZHANG, X. et al. Density Functional Theory Study on the Mechanism of Calcium Sulfate Reductive Decomposition by Carbon Monoxide. **Fuel**, v. 110, p. 204–211, 27 abr. 2012.

[30] KUMAR, A.; REDDY, S. N. Study the catalytic effect on pyrolytic behavior, thermal kinetic and thermodynamic parameters of Ni/Ru/Fe-impregnated sugarcane bagasse via thermogravimetric analysis. **Industrial Crops and Products**, v. 178, p. 114564, 2022.

[31] MOTAUNG, T. E.; ANANDJIWALA, R. D. Effect of alkali and acid treatment on thermal degradation kinetics of sugar cane bagasse. **Industrial Crops and Products**, v. 74, p. 472–477, 2015.

[32] ABOYADE, A. O. et al. Thermogravimetric study of the pyrolysis characteristics and kinetics of coal blends with corn and sugarcane residues. **Fuel Processing Technology**, v. 106, p. 310–320, 2013.

[33] HOTEIT, A. et al. Sulfate decomposition from circulating fluidized bed combustors bottom ash. **Chemical engineering science**, v. 62, n. 23, p. 6827–6835, 2007.

[34] MOSTASHARI, S. M.; BAGHI, O.; MOSTASHARI, S. Z. Thermogravimetric analysis of a cellulosic fabric treated with nickel sulfate hexahydrate as a flame retardant. **Cellulose Chemistry & Technology**, v. 43, n. 1, p. 95, 2009.

[35] DING, K. et al. Thermochemical reduction of magnesium sulfate by natural gas: insights from an experimental study. **Geochemical Journal**, v. 45, n. 2, p. 97–108, 2011.

[36] BROWNELL, W. E. Reactions Between Alkaline-Earth Sulfates and Cirstobalite. **Journal of the American Ceramic Society**, v. 46, n. 3, p. 125–128, 1963.

[37] KING, M. K.; MAHAPATRA, M. K. Thermal Decomposition of Nickel Salt Hydrates. **International Journal of Thermophysics**, v. 43, n. 3, p. 32, 2022.

[38] BALASUNDRAM, V. et al. Thermogravimetric kinetics of catalytic pyrolysis of sugarcane bagasse over nickel-cerium/HZSM-5 catalyst. **Journal of Advanced Research in Materials Science**, v. 64, n. 1, p. 1–17, 2020.

[39] PAPAZIAN, H. A.; PIZZOLATO, P. J.; ORRELL, R. R. The thermal decomposition of aluminum sulfate and hafnium sulfate. **Thermochimica Acta**, v. 4, n. 2, p. 97–103, 1972.

[40] PYSIAK, J.; GLINKA, A. Thermal decomposition of basic aluminium potassium sulfate. Part II. Kinetics of the reaction. **Thermochimica Acta**, v. 44, n. 1, p. 29–36, 1981.

[41] APTE, N. G. et al. Kinetic modeling of thermal decomposition of aluminum sulfate. **Chemical Engineering Communications**, v. 74, n. 1, p. 47–61, 1988.

[42] DISSERTATION, M. Julia Hernandez Cardoso Reductive decomposition of MgSO4 . 7H2O in the presence of H2 (g) Julia Hernandez Cardoso Reductive decomposition of MgSO4 . 7H2O in the presence of H2 (g). v. 2, n. December, 2018.

[43] VACHUŠKA, J.; VOBOŘIL, M. Kinetic data computation from non-isothermal thermogravimetric curves of non-uniform heating rate. **Thermochimica Acta**, v. 2, n. 5, p. 379–392, 1971.

[44] MELLO, N. M. et al. Effect of an alumina supported palladium catalyst on the magnesium sulfate decomposition kinetics. **Materials Research**, v. 23, p. e20200344, 2021.

[45] E SOUZA, B. M. **Thermodynamics Simulations and Kinetics Modeling of MgSO4. 7H2O Thermal Decomposition**. PUC-Rio, , 2022.

[46] SPEYER, R. **Thermal analysis of materials**. [s.l.] CRC press, 1993.

[47] RUEDA-ORDÓÑEZ, Y. J.; TANNOUS, K. Isoconversional kinetic study of the thermal decomposition of sugarcane straw for thermal

conversion processes. **Bioresource technology**, v. 196, p. 136–144, 2015.

[48] HUANG, Z. et al. Co-pyrolysis of poly (lactic acid) and sugar cane bagasse: Kinetic and thermodynamic studies. **Fuel**, v. 372, p. 132228, 2024.

[49] SPEYER, R. **Thermal analysis of materials**. [s.l.] CRC press, 1993.

[50] VACHUŠKA, J.; VOBOŘIL, M. Kinetic data computation from non-isothermal thermogravimetric curves of non-uniform heating rate. **Thermochimica Acta**, v. 2, n. 5, p. 379–392, 1971.

[51] NABLI, H. An overview on the simplex algorithm. **Applied Mathematics and Computation**, v. 210, n. 2, p. 479–489, 2009.

[52] MCKEE, D. W. Gasification of graphite in carbon dioxide and water vapor—the catalytic effects of alkali metal salts. **Carbon**, v. 20, n. 1, p. 59–66, 1982.

[53] MIAO, Q. et al. MgSO4-expanded graphite composites for mass and heat transfer enhancement of thermochemical energy storage. **Solar Energy**, v. 220, p. 432–439, 2021.

[54] TAO, Z. et al. Expanded graphite/polydimethylsiloxane composites with high thermal conductivity. **Journal of Applied Polymer Science**, v. 134, n. 21, 2017.

[55] SILVA, F. S. et al. Study of the thermal decomposition of mixtures sugarcane bagasse/titanium dioxide. **Journal of Thermal Analysis and Calorimetry**, v. 148, n. 1, p. 37–47, 2023.

[56] GARCÍA, R. et al. Biomass proximate analysis using thermogravimetry. **Bioresource technology**, v. 139, p. 1–4, 2013.

[57] MCKENDRY, P. Energy production from biomass (part 1): overview of biomass. **Bioresource technology**, v. 83, n. 1, p. 37–46, 2002.

[58] RAO, T. R.; SHARMA, A. Pyrolysis rates of biomass materials. **Energy**, v. 23, n. 11, p. 973–978, 1998.

[59] BAHÚ, J. O. et al. Kinetic study of thermal decomposition of sugarcane bagasse pseudo-components at typical pretreatment conditions: Simulations of opportunities towards the establishment of a

feasible primary biorefining. **Cleaner Chemical Engineering**, v. 4, p. 100074, 2022.

[60] MEMON, S. A. et al. Use of processed sugarcane bagasse ash in concrete as partial replacement of cement: mechanical and durability properties. **Buildings**, v. 12, n. 10, p. 1769, 2022.

[61] YANG, H. et al. Characteristics of hemicellulose, cellulose and lignin pyrolysis. **Fuel**, v. 86, n. 12–13, p. 1781–1788, 2007.

[62] LIU, Q. et al. Mechanism study of wood lignin pyrolysis by using TG–FTIR analysis. **Journal of analytical and applied pyrolysis**, v. 82, n. 1, p. 170–177, 2008.

[63] HLABELA, P. S. et al. Thermal reduction of barium sulphate with carbon monoxide—A thermogravimetric study. **Thermochimica acta**, v. 498, n. 1–2, p. 67–70, 2010.

[64] FRANKCOMBE, T. J.; SMITH, S. C. On the microscopic mechanism of carbon gasification: A theoretical study. **Carbon**, v. 42, n. 14, p. 2921–2928, 2004.

[65] FENG, B.; BHATIA, S. K. On the validity of thermogravimetric determination of carbon gasification kinetics. **Chemical Engineering Science**, v. 57, n. 15, p. 2907–2920, 2002.

[66] REIF, A. E. The mechanism of the carbon dioxide–carbon reaction. **The journal of physical chemistry**, v. 56, n. 6, p. 785–788, 1952.

[67] KURBAN, G. V. T. et al. Thermodynamics and kinetic modeling of the ZnSO4· H2O thermal decomposition in the presence of a Pd/Al2O3 catalyst. **Energies**, v. 15, n. 2, p. 548, 2022.

[68] HLABELA, P. S. et al. Thermal reduction of barium sulphate with carbon monoxide—A thermogravimetric study. **Thermochimica acta**, v. 498, n. 1–2, p. 67–70, 2010.

[69] KARIMI, A.; SEMAGINA, N.; GRAY, M. R. Kinetics of catalytic steam gasification of bitumen coke. **Fuel**, v. 90, n. 3, p. 1285–1291, 2011.

[70] RUEDA-ORDÓÑEZ, Y. J.; TANNOUS, K. Drying and thermal decomposition kinetics of sugarcane straw by nonisothermal thermogravimetric analysis. **Bioresource technology**, v. 264, p. 131–139, 2018.